

# Movable Antenna-enabled RIS-aided Integrated Sensing and Communication

Haisu Wu, Hong Ren, *Member, IEEE*, Cunhua Pan, *Senior Member, IEEE*

**Abstract**—In this paper, we investigate a movable antenna (MA)-aided integrated sensing and communication (ISAC) system, where a reconfigurable intelligent surface (RIS) is employed to enhance wireless communication and sensing performance in dead zones. Specifically, this paper aims to maximize the minimum beampattern gain at the RIS by jointly optimizing beamforming matrix at the base station (BS), the reflecting coefficients at the RIS and the positions of the MAs, subject to signal-to-interference-plus-noise ratio (SINR) constraint for the users and maximum transmit power at the BS. To tackle this non-convex optimization problem, we propose an alternating optimization (AO) algorithm and employ semidefinite relaxation (SDR), sequential rank-one constraint relaxation (SRCR) and successive convex approximation (SCA) techniques. Numerical results indicate that the MA and RIS-aided ISAC system outperforms conventional fixed position antenna (FPA) and RIS-aided systems. In addition, the application of MAs can reduce the similarity of user channels and enhance channel gain in the ISAC system.

**Index Terms**—Movable antenna (MA), integrated sensing and communication (ISAC), reconfigurable intelligent surface (RIS), antenna position optimization.

## I. INTRODUCTION

**F**UTURE sixth generation (6G) communication is anticipated to support applications such as Massive Internet of Things (Massive-IoT), industrial automation (IA), and virtual reality (VR), which demand higher sensing precision and lower communication latency. These demands for 6G technologies call for a paradigm shift in the existing wireless communication networks. In particular, integrated sensing and communication (ISAC) is regarded as one of the key transformative technologies for future 6G networks [1]–[4]. The objective of ISAC is to consolidate the sensing and communication functions onto a unified platform which allows for the sharing of resources, hardware facilities, and signal-processing modules, thereby enhancing both spectrum and hardware efficiency. In addition, millimeter-wave (mmW)/Terahertz (THz) signals [5] and ultra-massive MIMO [6] are expected to be utilized in the future communication system, implying that future wireless communication and radar sensing systems will become similar in hardware, which further enables the sharing of hardware resources.

Based on the aforementioned background, Dual-functional radar and communication (DFRC) is proposed as a paradigm of ISAC systems, which perform both sensing and communication functions with shared frequency spectrum on an identical hardware platform [7]–[9]. Compared with another frame-

work of ISAC, namely radar and communication coexistence (RCC), the integration of DFRC can reduce hardware costs and simplify design complexity. Currently, DFRC has received increasing attention, and most of the related investigations considered the beamforming design at the DFRC base station (BS). For instance, the authors of [1] initially considered the beampattern design in a DFRC system. Specifically, the spatial beamforming waveform at the DFRC BS is optimized to minimize the power of the interference for downlink communication users, subject to several design criteria of the radar. In addition, the authors of [10] investigated the beamforming design of a co-located MIMO system with a monostatic DFRC radar. Specifically, the authors proposed the simultaneous transmission of radar waveforms and communication symbols, which can form multiple beams and better exploits the degrees of freedom (DoFs) in the MIMO system. Based on the aforementioned works, the authors of [11] considered the transmit beamforming in a downlink ISAC system to enhance the radar sensing performance while guaranteeing the user SINR constraint. In particular, the authors investigated the impact of whether the receivers could cancel the interference from dedicated radar signals on sensing performance. Nevertheless, although mmW/THz signals can provide extensive bandwidth which is capable of enhancing the communication and sensing performance, the high frequency will lead to increased susceptibility of the transmit signal to be obstructed. In scenarios where the line-of-sight (LoS) links between the DFRC BS and the targets are obstructed, the performance of the ISAC system will experience substantial degradation.

Reconfigurable intelligent surface (RIS) is considered as a promising technology to address the aforementioned challenges [12]–[15]. An RIS is a meta-surface consisting of passive reflecting elements, each of which is capable of independently altering the phase of incident signals. Therefore, the RIS can intelligently reconstruct the wireless channels, thereby strengthening the quality of service (QoS) of the legitimate users. In terms of the sensing function, RIS can also establish virtual LoS links in dead zones of the DFRC BS, significantly improving sensing capabilities in the ISAC systems [16]–[19]. For instance, the authors of [16] jointly optimized the transmit beamforming and the phase shift of the RIS to maximize the sensing SINR for a single target of interest at the BS subject to various communication constraints. In [17], transmit beamforming at the BS and reflecting phase shifts of the RIS were jointly optimized to maximize the minimum beampattern gain towards the desired direction in the NLoS area of the BS subject to a single user's communication SINR constraint. Furthermore, the authors of [18] proposed the novel scheme of

using two dedicated RISs for enhancing communication and sensing tasks respectively. They also demonstrated that the sensing performance can be greatly enhanced when the target is located at the NLoS area of the BS.

Nonetheless, in the aforementioned ISAC systems, the MIMO architectures generally utilized fixed-position antenna (FPA) arrays, which restrict the full utilization of the available DoFs within the continuous spatial domain, thereby hindering optimal spatial diversity and multiplexing performance in communication and sensing tasks. Furthermore, the unchangeable geometric configurations of conventional FPA arrays, can lead to certain array gain loss during radar beamforming tasks.

Recently, the novel concept of movable antenna (MA) has been proposed as an innovative solution to overcome the inherent limitations in FPA systems [20]–[22]. Unlike traditional FPAs, each antenna in MA systems is linked to a radio frequency (RF) chain through a flexible cable [22]. By facilitating a driver component or similar mechanisms, the positions of MAs can be adjusted dynamically within a designated spatial area, thereby reconstructing channel conditions to boost communication performance, or reconfiguring the geometric properties of the MIMO arrays to enhance sensing capability. Channel modeling for MA-aided communication systems was initially explored in [21], where the authors introduced a field-response channel model applicable under far-field conditions. They conducted a comparative performance analysis of MA-aided and FPA systems across deterministic and statistical channels, highlighting the substantial advantages in enhancing received power and reducing outage probability of the MA-aided system. Additionally, the approximate cumulative distribution function (CDF) for the maximum channel gain was derived in closed form, providing a valuable tool for evaluating the outage probability of the MA-aided communication system. In [23], [24], the research explored channel estimation for MA-aided communication systems by using compressed sensing method. Based on perfect channel state information (CSI), extensive research has shown that MA-aided systems provide substantial improvements over traditional FPA systems in wireless communication [25]–[34]. For example, MA-aided multi-terminal uplink transmission system with an FPA BS was investigated in [25], where power minimization problem was formulated subject to minimum-achievable-rate of terminals and a gradient descent-based iterative method was proposed to optimize the positions of MAs. In addition, the MA-aided full-duplex (FD) wireless system was studied in [34], where MAs are deployed at both the transmitter and receiver. The PPSO algorithm was devised to optimize the positions of MAs, and numerical results demonstrated the superior performance of the MA-FD system over the FPA-FD system.

Nevertheless, the potential of MA in the field of wireless sensing has not yet been fully explored, and only a few existing studies considered wireless sensing without communication [35], [36]. The authors of [35] investigated the enhanced multi-beam forming with a linear MA array by optimizing antenna positions to exploit new DoFs. In addition, in [36], the authors delved into both one-dimensional (1D) and two-dimensional (2D) MA arrays and demonstrated that the MA

array can greatly improve sensing capacity of the system over its FPA counterparts both analytically and numerically. Notably, numerical simulations revealed lower correlation of the steering vectors for 1D/2D MA arrays, which can enhance wireless sensing performance. Furthermore, the authors of [37] introduced linear 1D MAs into ISAC system, and then considered relatively simple settings where the transmit beamforming at the BS and the positions of the MAs were jointly optimized to maximize the communication rate and sensing mutual information. Nevertheless, these studies all considered the LoS links between the BS and the targets. In contrast, if the targets may locate in the NLoS area of the BS, it is reasonable to apply an RIS to enhance the sensing performance of the MA-aided system.

Against the above background, this paper considers an ISAC system which is assisted by a 2D MA array and an RIS for effective wireless sensing and communication in dead zones. The main contributions of our paper are summarized as follows:

- We consider an MA and RIS-aided ISAC system, where a DFRC BS equipped with a 2D MA array aims to sense the targets located in multiple angles and serve the communication users. In particular, the angles of interest are located in the NLoS area of the DFRC BS, thus an RIS is deployed to create a virtual LoS link to enhance the wireless sensing and communication performance. Then, we formulate the minimum beampattern gain maximization problem subject to communication SINR constraints.
- To address this highly non-convex optimization problem, we propose an AO-based algorithm which incorporates several techniques: successive convex approximation (SCA), semidefinite relaxation (SDR) and sequential rank-one constraint relaxation (SRCR). Specifically, we optimize the transmit beamforming at the BS by using SDR and the phase shifts at the RIS by using the SRCR algorithm to avoid potential non-convergence issues of SDR. For the tightly coupled positions of MAs, we iteratively optimize individual antenna positions by using the SCA algorithm while fixing the positions of other antennas to obtain a suboptimal solution.
- Simulation results confirm the performance improvement of deploying MAs in RIS-aided ISAC systems compared to FPAs. In addition, the application of MAs can reduce the similarity of user channels in ISAC systems, thereby effectively mitigating multi-user interference. Furthermore, antenna displacement can alleviate multipath effects caused by channel fading and enhance channel gain.

*Notations:* Boldface lower case and upper case letters denote vectors and matrices, respectively.  $(\cdot)^*$ ,  $(\cdot)^T$  and  $(\cdot)^H$  denote the conjugate, transpose and conjugate transpose (Hermitian), respectively.  $\mathbb{E}[\cdot]$  denotes the expectation operation.  $\|\mathbf{a}\|_2$  denotes the 2-norm of vector  $\mathbf{a}$ . The set of  $P \times Q$  complex and real matrices is denoted by  $\mathbb{C}^{P \times Q}$  and  $\mathbb{R}^{P \times Q}$ , respectively. We use  $[A]_{p,q}$  to denote the entry of matrix  $A$  in its  $p$ -th row and  $q$ -th column.  $\Re\{\mathbf{a}\}$  denotes the real part of vector  $\mathbf{a}$ .  $\text{diag}(\mathbf{a})$  denotes a square diagonal matrix with the elements of vector  $\mathbf{a}$  as its diagonal elements, while  $\text{diag}(A)$  denotes

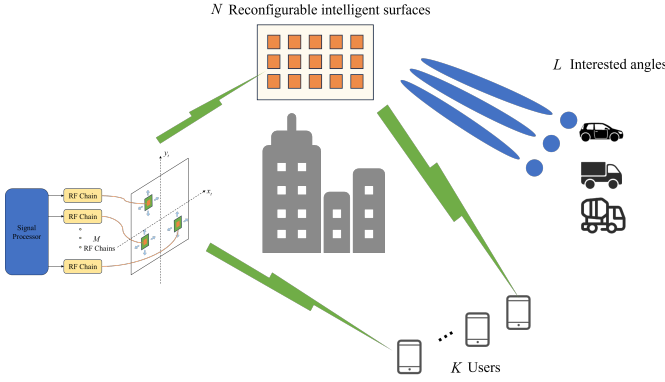


Fig. 1: MA and RIS-aided ISAC system.

a column vector consisting of the main diagonal elements of matrix  $\mathbf{A}$ .  $\mathbf{A} \succeq 0$  indicates that  $\mathbf{A}$  is a positive semidefinite matrix.  $\mathcal{CN}(0, \sigma^2)$  denotes the circularly symmetric complex Gaussian (CSCG) distribution with zero mean and covariance  $\sigma^2$ .  $\text{rank}(\mathbf{A})$  denotes the rank of matrix  $\mathbf{A}$ . The amplitude and phase of complex value  $a$  are denoted by  $|a|$  and  $\angle a$ , respectively.

## II. SYSTEM MODEL

We consider an MA and RIS-aided ISAC system as depicted in Fig. 1, where a DFRC BS equipped with a uniform linear array (ULA) of  $M$  antennas serves  $K$  single-antenna users and detects targets located in the NLoS area of the DFRC BS. In addition, an RIS with  $N$  reflecting elements is deployed in the system to enhance the communication and sensing performance, and it is assumed that the targets are located at  $L$  interested angles towards the RIS.

### A. Signal Model

The transmit signal of the DFRC BS is represented as

$$\mathbf{x} = \mathbf{W}_r \mathbf{s} + \mathbf{W}_c \mathbf{c} = [\mathbf{W}_r, \mathbf{W}_c] [\mathbf{s}^T, \mathbf{c}^T]^T = \mathbf{W} \tilde{\mathbf{x}}, \quad (1)$$

where  $\mathbf{s} \in \mathbb{C}^{M \times 1}$  is the radar signal, and  $\mathbf{c} \in \mathbb{C}^{K \times 1}$  denotes the transmit symbols to the  $K$  users. In addition,  $\mathbf{W}_r = [\mathbf{w}_{r,1}, \mathbf{w}_{r,2}, \dots, \mathbf{w}_{r,M}] \in \mathbb{C}^{M \times M}$ ,  $\mathbf{W}_c = [\mathbf{w}_{c,1}, \mathbf{w}_{c,2}, \dots, \mathbf{w}_{c,K}] \in \mathbb{C}^{M \times K}$  denote the beamforming matrices for radar and communication, respectively.  $\mathbf{W} = [\mathbf{W}_r, \mathbf{W}_c] \in \mathbb{C}^{M \times (M+K)}$  represents the equivalent DFRC transmit beamforming matrix. It is assumed that the radar signals are generated by pseudo-random coding, which satisfies  $\mathbb{E}[\mathbf{s}] = \mathbf{0}$  and  $\mathbb{E}[\mathbf{s}\mathbf{s}^H] = \mathbf{I}_M$ . The communication signal  $\mathbf{c}$  is assumed to follow  $\mathcal{CN}(\mathbf{0}, \mathbf{I}_K)$ , and the radar and communication signals are uncorrelated. Therefore, the covariance matrix of the transmit signal can be expressed as

$$\mathbf{R} = \mathbb{E}[\mathbf{x}\mathbf{x}^H] = \mathbf{W}\mathbf{W}^H = \mathbf{W}_r\mathbf{W}_r^H + \sum_{k=1}^K \mathbf{R}_k, \quad (2)$$

where the rank-1 matrix  $\mathbf{R}_k$  is introduced by  $\mathbf{R}_k \triangleq \mathbf{w}_{c,k}\mathbf{w}_{c,k}^H$ .

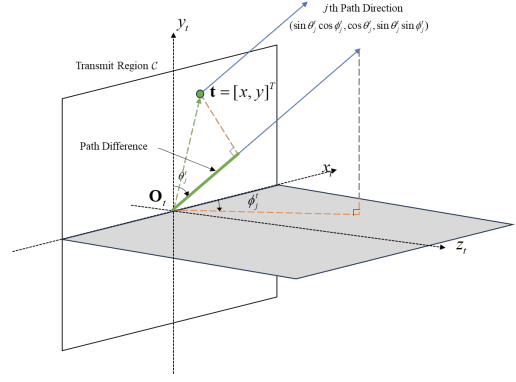


Fig. 2: Illustration of the coordinates and spatial angles in transmit region.

### B. Channel Model

This paper utilizes the planar far-field response model in [21], where each channel transmission component has the same AoD, AoA, and path response coefficient, but different signal phases. Specifically, let us define  $\tilde{\mathbf{t}} = [\mathbf{t}_1, \mathbf{t}_2, \dots, \mathbf{t}_M]^T \in \mathbb{R}^{2 \times M}$  as the positions of MAs at the BS, where  $\mathbf{t}_m = [x_m, y_m]^T \in \mathcal{C}$ ,  $1 \leq m \leq M$  represents the coordinates of the  $m$ -th MA, and  $\mathcal{C}$  is the transmit region of the MAs.

As shown in Fig. 2, the elevation and azimuth angles of the transmit area and the receive area are denoted as  $\theta_j^t \in [0, \pi]$ ,  $\phi_j^t \in [0, \pi]$ ,  $1 \leq j \leq L_t$  and  $\theta_i^r \in [0, \pi]$ ,  $\phi_i^r \in [0, \pi]$ ,  $1 \leq i \leq L_r$ , respectively. Here,  $L_t$  is the number of transmit paths from the BS to the RIS, and  $L_r$  is the number of receive paths at the RIS, respectively. In addition, the number of transmit paths for the direct channel from the BS to the  $k$ -th user is defined as  $L_k^t$ ,  $1 \leq k \leq K$ . For the MA-aided system, the channel matrix is determined by the signal propagation environment and the MAs' position. According to [21], the field response vector (FRV) of the MA at position  $\mathbf{t} = [x, y]^T$  in the BS-RIS link is given by:

$$\mathbf{g}(\mathbf{t}) = \left[ e^{j\frac{2\pi}{\lambda}\rho_t^1(\mathbf{t})}, e^{j\frac{2\pi}{\lambda}\rho_t^2(\mathbf{t})}, \dots, e^{j\frac{2\pi}{\lambda}\rho_t^{L_t}(\mathbf{t})} \right]^T \in \mathbb{C}^{L_t}, \quad (3)$$

where  $\lambda$  represents the wavelength and  $\rho_t^j(\mathbf{t}) = x \sin \theta_j^t \cos \phi_j^t + y \cos \theta_j^t$  represents the path difference of the  $j$ -th path at position  $\mathbf{t}$  compared to the reference origin. Therefore, the field response matrix (FRM) of the BS-RIS link for all  $M$  transmit MAs is given by:

$$\mathbf{G}(\tilde{\mathbf{t}}) \triangleq [\mathbf{g}(\mathbf{t}_1), \mathbf{g}(\mathbf{t}_2), \dots, \mathbf{g}(\mathbf{t}_M)] \in \mathbb{C}^{L_t \times M}. \quad (4)$$

Similarly, the FRM of the BS-User link for all  $M$  MAs is:

$$\mathbf{G}_k(\tilde{\mathbf{t}}) \triangleq [\mathbf{g}_k(\mathbf{t}_1), \mathbf{g}_k(\mathbf{t}_2), \dots, \mathbf{g}_k(\mathbf{t}_M)] \in \mathbb{C}^{L_k^t \times M}, 1 \leq k \leq K. \quad (5)$$

In addition, it can be derived that the FRV for a single reflecting element at the RIS is

$$\mathbf{f}(\mathbf{r}) = \left[ e^{j\frac{2\pi}{\lambda}\rho_r^1(\mathbf{r})}, e^{j\frac{2\pi}{\lambda}\rho_r^2(\mathbf{r})}, \dots, e^{j\frac{2\pi}{\lambda}\rho_r^{L_r}(\mathbf{r})} \right]^T \in \mathbb{C}^{L_r}, \quad (6)$$

where  $\rho_r^i(\mathbf{r}) = x \sin \theta_i^r \cos \phi_i^r + y \cos \theta_i^r$  is the difference of the signal propagation distance for the  $i$ -th receive path between

position  $\mathbf{r}$  and the origin of the RIS. Hence, the FRM at the RIS is represented as

$$\mathbf{F}(\mathbf{r}) = [\mathbf{f}(\mathbf{r}_1), \mathbf{f}(\mathbf{r}_2), \dots, \mathbf{f}(\mathbf{r}_N)] \in \mathbb{C}^{L_r \times N}. \quad (7)$$

Then, let us denote the path response matrix (PRM)  $\mathbf{\Sigma} \in \mathbb{C}^{L_r \times L_t}$  and  $\mathbf{\Sigma}_k \in \mathbb{C}^{L_r^k \times L_t^k}$ ,  $1 \leq k \leq K$  as the responses of all transmit and receive paths from the BS to the RIS and from the BS to the  $k$ -th user, respectively. Therefore, the channel matrix from the BS to the RIS can be expressed as:

$$\mathbf{H}(\tilde{\mathbf{t}}) = \mathbf{F}(\mathbf{r})^H \mathbf{\Sigma} \mathbf{G}(\tilde{\mathbf{t}}). \quad (8)$$

Similarly, the channel from the BS to the  $k$ -th user can be given by

$$\mathbf{h}_{1,k}^H(\tilde{\mathbf{t}}) = \mathbf{1}^H \mathbf{\Sigma}_k \mathbf{G}_k(\tilde{\mathbf{t}}) \in \mathbb{C}^{1 \times M}. \quad (9)$$

Assume that all users are equipped with a single antenna and the positions of the reflecting elements in the RIS are fixed, the channel matrix from the RIS to the  $k$ -th user can be represented as  $\mathbf{h}_{2,k} \in \mathbb{C}^{N \times 1}$ .

We assume that the channel state information (CSI) of the channels is perfectly known at the DFRC BS with the application of MA-related channel estimation methods [23], [24].

### III. PROBLEM FORMULATION

#### A. Communication Metric

By combining the signals from both BS-UE and BS-RIS-UE links, the received signal at the  $k$ -th user is

$$y_k = (\mathbf{h}_{2,k}^H \mathbf{\Phi} \mathbf{H}(\tilde{\mathbf{t}}) + \mathbf{h}_{1,k}^H(\tilde{\mathbf{t}})) \mathbf{x} + n_k, \quad (10)$$

where  $n_k \sim \mathcal{CN}(0, \sigma_k^2)$  denotes additive white Gaussian noise (AWGN) at the  $k$ -th user receiver with covariance of  $\sigma_k^2$ . Thus, the SINR for the  $k$ -th user is

$$\begin{aligned} \text{SINR}_k &= \frac{\mathbf{h}_k^H \mathbf{w}_k \mathbf{w}_k^H \mathbf{h}_k}{\sum_{1 \leq i \leq M+K, i \neq k} \mathbf{h}_k^H \mathbf{w}_i \mathbf{w}_i^H \mathbf{h}_k + \sigma_k^2} \\ &= \frac{\mathbf{h}_k^H \mathbf{R}_k \mathbf{h}_k}{\sum_{1 \leq i \leq M+K, i \neq k} \mathbf{h}_k^H \mathbf{R}_i \mathbf{h}_k + \sigma_k^2} \\ &= \frac{\mathbf{h}_k^H \mathbf{R}_k \mathbf{h}_k}{\mathbf{h}_k^H (\mathbf{R} - \mathbf{R}_k) \mathbf{h}_k + \sigma_k^2}, \end{aligned} \quad (11)$$

where  $\mathbf{h}_k^H \triangleq \mathbf{h}_{2,k}^H \mathbf{\Phi} \mathbf{H}(\tilde{\mathbf{t}}) + \mathbf{h}_{1,k}^H(\tilde{\mathbf{t}})$  represents the equivalent channel between the BS and the  $k$ -th user.

#### B. Radar Sensing Metrics

Next, we consider the perception of potential targets in the NLoS area of BS. In this case, since the potential targets are located in the NLoS area of the BS, and we assume that the virtual LoS channels created by the RIS are much stronger than the NLoS ones. Hence, the effect of NLoS channel between the BS and sensing targets can be neglected. In addition, it is assumed that the location of the RIS is well designed with few obstacles. Therefore, we adopt the beam direction gain of the RIS at the desired sensing angle as the sensing performance metrics. Let  $d_{\text{RIS}}$  represent the spacing between consecutive reflective elements at the RIS, and  $\lambda$  represent the wavelength.

Therefore, the steering vector at the RIS for the AoD  $\theta$  is given by

$$\mathbf{a}(\theta) = \left[ 1, e^{j \frac{2\pi d_{\text{RIS}}}{\lambda} \sin \theta}, \dots, e^{j \frac{2\pi (N-1) d_{\text{RIS}}}{\lambda} \sin \theta} \right]^T. \quad (12)$$

As in [10], we consider that both the signal symbol  $\mathbf{c}$  and the radar symbol  $\mathbf{s}$  can be used for sensing objects. Therefore, the beampattern gain at the RIS corresponding to angle  $\theta$  is

$$\begin{aligned} \mathcal{P}(\theta) &= \mathbb{E} \left( \left| \mathbf{a}^H(\theta) \mathbf{\Phi} \mathbf{H}(\tilde{\mathbf{t}}) (\mathbf{W}_r \mathbf{s} + \mathbf{W}_c \mathbf{s}) \right|^2 \right) \\ &= \mathbf{a}^H(\theta) \mathbf{\Phi} \mathbf{H}(\tilde{\mathbf{t}}) \mathbf{R} \mathbf{H}(\tilde{\mathbf{t}})^H \mathbf{\Phi}^H \mathbf{a}(\theta). \end{aligned} \quad (13)$$

We are interested in specific  $L$  angles  $\{\theta_1, \dots, \theta_L\}$ , and we define  $\mathcal{L} \triangleq \{1, \dots, L\}$  as the set of sensing angles of interest.

#### C. Optimization Problem

In this paper, we aim to maximize the minimum beampattern gain in the directions of the  $L$  interested sensing angles by jointly optimizing the covariance matrix  $\mathbf{R}$  of the transmit beamformer at the BS, the phase shifts  $\mathbf{\Phi}$  at the RIS, and the positions  $\tilde{\mathbf{t}}$  of the MAs. Accordingly, the problem is formulated as

$$\max_{\mathbf{R}, \mathbf{\Phi}, \tilde{\mathbf{t}}} \min_{l \in \mathcal{L}} \mathbf{a}^H(\theta_l) \mathbf{\Phi} \mathbf{H}(\tilde{\mathbf{t}}) \mathbf{R} \mathbf{H}(\tilde{\mathbf{t}})^H \mathbf{\Phi}^H \mathbf{a}(\theta_l) \quad (14)$$

$$\text{s.t. SINR}_k \geq \Gamma, \quad \forall k, \quad (14a)$$

$$\text{tr}(\mathbf{R}) \leq P_0, \quad (14b)$$

$$\mathbf{R} \succeq 0, \quad (14c)$$

$$\text{rank}(\mathbf{R}_k) = 1 \quad (14d)$$

$$\mathbf{\Phi} = \text{diag}(e^{j\phi_1}, \dots, e^{j\phi_N}), \quad (14e)$$

$$\|\mathbf{t}_k - \mathbf{t}_q\|_2 \geq D, \quad k \neq q, \quad (14f)$$

$$\tilde{\mathbf{t}} \in \mathcal{C}, \quad (14g)$$

where  $P_0$  denotes the maximum transmit power at the BS,  $\Gamma$  denotes the minimum SINR threshold of the users, and  $D$  represents the minimum distance between MAs to prevent coupling effects.

It is challenging to solve Problem (14) due to the intricately coupled variables  $\mathbf{R}$ ,  $\mathbf{\Phi}$ ,  $\tilde{\mathbf{t}}$ . Furthermore, the objective function of Problem (14) exhibits non-smooth characteristics, and the channel vectors are highly non-convex with respect to MA positions  $\tilde{\mathbf{t}}$ , which increases the difficulty of solving Problem (14).

## IV. PROPOSED AO-BASED ALGORITHM

#### A. Transmit Beamforming Optimization at the BS

In this subsection, we optimize the beamforming matrix  $\mathbf{R}$  at the DFRC BS with fixed  $\mathbf{\Phi}$  and  $\tilde{\mathbf{t}}$ . According to the requirements of the SINR (14a), we can transform the SINR constraint into the following form

$$(1 + \Gamma^{-1}) \text{tr}(\mathbf{R}_k \mathbf{H}_k) \geq \text{tr}(\mathbf{R} \mathbf{H}_k) + \sigma_k^2, \quad k = 1, \dots, K, \quad (15)$$

where  $\mathbf{H}_k = \mathbf{h}_k \mathbf{h}_k^H$ . As a result, (14) becomes the optimization of  $\mathbf{R}$  in the following form:

$$\max_{\mathbf{R}} \min_{l \in \mathcal{L}} \mathbf{a}^H(\theta_l) \Phi \mathbf{H}(\tilde{\mathbf{t}}) \mathbf{R} \mathbf{H}(\tilde{\mathbf{t}})^H \Phi^H \mathbf{a}(\theta_l) \quad (16a)$$

$$\text{s.t.} \quad (1 + \Gamma^{-1}) \text{tr}(\mathbf{R}_k \mathbf{H}_k) \geq \text{tr}(\mathbf{R} \mathbf{H}_k) + \sigma_k^2, \quad (16b)$$

$$\text{tr}(\mathbf{R}) \leq P_0, \quad (16c)$$

$$\mathbf{R} \succeq 0, \quad (16d)$$

$$\text{rank}(\mathbf{R}_k) = 1. \quad (16e)$$

Owing to the rank-one constraint (16e), the optimization problem is still non-convex. To handle this problem, we utilize the key idea of the SDR method. By omitting the rank-one constraints, Problem (16) can be recast as

$$\max_{\mathbf{R}, \{\mathbf{R}_k\}} \min_{l \in \mathcal{L}} \text{tr}(\mathbf{A}(\theta_l) \mathbf{R}) \quad (17a)$$

$$\text{s.t.} \quad (1 + \Gamma^{-1}) \text{tr}(\mathbf{R}_k \mathbf{H}_k) \geq \text{tr}(\mathbf{R} \mathbf{H}_k) + \sigma_k^2, \quad (17b)$$

$$\text{tr}(\mathbf{R}) \leq P_0, \quad (17c)$$

$$\mathbf{R} \succeq 0, \quad (17d)$$

$$\mathbf{R} - \sum_{k=1}^K \mathbf{R}_k \succeq 0, \quad (17e)$$

where  $\mathbf{A}(\theta_l) = \mathbf{H}(\tilde{\mathbf{t}})^H \Phi^H \mathbf{a}(\theta_l) \mathbf{a}^H(\theta_l) \Phi \mathbf{H}(\tilde{\mathbf{t}})$  is independent of  $\mathbf{R}$ . Problem (17) is a convex SDP problem where all the constraints are either linear or semidefinite and the global optimal point can be obtained in polynomial time by using the convex optimization toolbox, CVX [38]. Denote  $\hat{\mathbf{R}}, \{\hat{\mathbf{R}}_k\}$  as a feasible solution to Problem (17), we can construct the optimal rank-one solution  $\tilde{\mathbf{R}}, \{\tilde{\mathbf{R}}_k\}$  to Problem (16), as shown in Appendix A.

### B. Reflective Beamforming Optimization

In this subsection, we optimize the phase shift  $\Phi$  of the RIS, with fixed covariance matrix  $\mathbf{R}$  of transmit signal and fixed position  $\tilde{\mathbf{t}}$  of  $M$  MAs. The subproblem can be rewritten as

$$\max_{\Phi} \min_{l \in \mathcal{L}} \mathbf{a}^H(\theta_l) \Phi \mathbf{H}(\tilde{\mathbf{t}}) \mathbf{R} \mathbf{H}(\tilde{\mathbf{t}})^H \Phi^H \mathbf{a}(\theta_l) \quad (18a)$$

$$\text{s.t.} \quad \text{SINR}_k \geq \Gamma, \forall k, \quad (18b)$$

$$\Phi = \text{diag}(e^{j\phi_1}, \dots, e^{j\phi_N}). \quad (18c)$$

We first define  $\mathbf{v} \triangleq \text{vec}(\Phi^*) = [e^{j\phi_1}, \dots, e^{j\phi_N}]^H$  and introduce the following definition

$$\mathbf{H}_l \triangleq \text{diag}(\boldsymbol{\alpha}(\theta_l)^H) \mathbf{H}(\tilde{\mathbf{t}}) \mathbf{R} \mathbf{H}(\tilde{\mathbf{t}})^H \text{diag}(\boldsymbol{\alpha}(\theta_l)), \quad \forall l \in \mathcal{L}. \quad (19)$$

Then the beampattern gain towards angle  $\theta$  is rewritten as

$$\mathcal{P}(\theta) = \mathbf{v}^H \mathbf{H}_l \mathbf{v}. \quad (20)$$

Then, by letting  $\mathbf{G}_k = \text{diag}(\mathbf{h}_{1,k}^H) \mathbf{H}(\tilde{\mathbf{t}})$ , the SINR constraint in (18a) is reformulated as

$$(\mathbf{v}^H \mathbf{G}_k + \mathbf{H}_{2,k}^H) \tilde{\mathbf{R}}_k (\mathbf{G}_k^H \mathbf{v} + \mathbf{H}_{2,k}) \geq \sigma^2, \quad (21)$$

where  $\tilde{\mathbf{R}}_k = (1 + \Gamma^{-1}) \mathbf{R}_k - \mathbf{R}$ . In addition, (20) can be further recast as

$$\bar{\mathbf{v}}^H \mathbf{W}_k \bar{\mathbf{v}} \geq \sigma_k^2, \quad (22)$$

with

$$\mathbf{W}_k = \begin{bmatrix} \mathbf{G}_k \tilde{\mathbf{R}}_k \mathbf{G}_k^H & \mathbf{G}_k \tilde{\mathbf{R}}_k \mathbf{H}_{2,k} \\ \mathbf{H}_{2,k}^H \tilde{\mathbf{R}}_k \mathbf{G}_k^H & \mathbf{H}_{2,k}^H \tilde{\mathbf{R}}_k \mathbf{H}_{2,k} \end{bmatrix}, \quad \bar{\mathbf{v}} = \begin{bmatrix} \mathbf{v} \\ 1 \end{bmatrix}. \quad (23)$$

For further manipulations, let us define

$$\bar{\mathbf{H}}_l = \begin{bmatrix} \mathbf{H}_l & \mathbf{0}_{N \times 1} \\ \mathbf{0}_{1 \times N} & 0 \end{bmatrix}, \quad (24)$$

and by substituting (23) (24) into (20), we have  $\mathcal{P}(\theta) = \bar{\mathbf{v}}^H \bar{\mathbf{H}}_l \bar{\mathbf{v}}$ . Hence, Problem (18) with the fixed transmit covariance matrix  $\mathbf{R}$  and fixed position  $\tilde{\mathbf{t}}$  of  $M$  MAs can be recast as

$$\max_{\bar{\mathbf{v}}} \min_{l \in \mathcal{L}} \bar{\mathbf{v}}^H \bar{\mathbf{H}}_l \bar{\mathbf{v}} \quad (25a)$$

$$\text{s.t.} \quad \bar{\mathbf{v}}^H \mathbf{W}_k \bar{\mathbf{v}} \geq \sigma^2, \quad \forall k, \quad (25b)$$

$$|\bar{v}_n| = 1, \forall n \in \{1, \dots, N + 1\}, \quad (25c)$$

which is still non-convex, due to the unit-modulus constraints of (25c). To address this issue, we define  $\bar{\mathbf{V}} = \bar{\mathbf{v}} \bar{\mathbf{v}}^H$  and (25) is reformulated as

$$\max_{\bar{\mathbf{v}}} \min_{l \in \mathcal{L}} \text{tr}(\bar{\mathbf{H}}_l \bar{\mathbf{V}}) \quad (25)$$

$$\text{s.t.} \quad \text{tr}(\mathbf{W}_k \bar{\mathbf{V}}) \geq \sigma^2, \forall k, \quad (26a)$$

$$\bar{V}_{n,n} = 1, \forall n \in \{1, \dots, N + 1\}, \quad (26b)$$

$$\bar{\mathbf{V}} \succeq 0, \quad (26c)$$

$$\text{rank}(\bar{\mathbf{V}}) = 1. \quad (26d)$$

The only non-convex constraint is the rank-one constraint (26d) in (26), which can be typically addressed by using the SDR and Gaussian randomization technique. However, in the case of strict constraints, as in Problem (26), the approximation methods such as Gaussian randomization algorithm cannot guarantee the convergence of the overall algorithm [19]. Therefore, we adopt SRCR to convert (26d) equivalently to [39]

$$\mathbf{u}_{\max}^H(\bar{\mathbf{V}}^{(t)}) \bar{\mathbf{V}} \mathbf{u}_{\max}(\bar{\mathbf{V}}^{(t)}) \geq w^{(t)} \text{Tr}(\bar{\mathbf{V}}), \quad (27)$$

where  $\bar{\mathbf{V}}^{(t)}$  is a feasible solution obtained in the  $t$ -th iteration,  $\mathbf{u}_{\max}(\bar{\mathbf{V}}^{(t)})$  is the eigenvector corresponding to the maximum eigenvalue of  $\bar{\mathbf{V}}^{(t)}$ ,  $w^{(t)}$  denotes a relaxation parameter which will gradually approach 1. Finally, our optimization problem in the  $t$ -th iteration is given by

$$\max_{\bar{\mathbf{V}}} \min_{l \in \mathcal{L}} \text{tr}(\bar{\mathbf{H}}_l \bar{\mathbf{V}}) \quad (28a)$$

$$\text{s.t.} \quad \text{tr}(\mathbf{W}_k \bar{\mathbf{V}}) \geq \sigma^2, \quad \forall k, \quad (28b)$$

$$\bar{V}_{n,n} = 1, \forall n \in \{1, \dots, N + 1\}, \quad (28c)$$

$$\bar{\mathbf{V}} \succeq 0, \quad (28d)$$

$$\mathbf{u}_{\max}^H(\bar{\mathbf{V}}^{(t)}) \bar{\mathbf{V}} \mathbf{u}_{\max}(\bar{\mathbf{V}}^{(t)}) \geq w^{(t)} \text{Tr}(\bar{\mathbf{V}}). \quad (28e)$$

---

**Algorithm 1** SRCR Algorithm for Optimizing RIS Coefficients
 

---

1: **Input:**  $\{\bar{\mathbf{H}}_l\}_{l=1}^L, \{\mathbf{W}_k\}_{k=1}^K$ .  
 2: Initialize  $\{\mathbf{t}_m\}_{m=1}^M, w^{(0)} = 0, \tau^{(0)}$ .  
 3: **while**  $\text{Tr}(\bar{\mathbf{V}}^{(t)}) / \lambda_{\max}(\bar{\mathbf{V}}^{(t)}) - 1$  is above  $\epsilon$  **do**  
 4:   **if** Problem (28) is solvable with  $\mathbf{V}^{(t)}$  and  $w^{(t)}$  **then**  
 5:     Obtain  $\bar{\mathbf{V}}^{(t+1)}$  by solving Problem (28),  $\tau^{(t+1)} = \tau^{(t)}$   
 6:   **else**  
 7:     Update  $\bar{\mathbf{V}}^{(t+1)} = \bar{\mathbf{V}}^{(t)}$ ;  
 8:     Update  $\tau^{(t+1)} = \tau^{(t)} / 2$ ;  
 9:   **end if**  
 10:  $w^{(t+1)} = \min\left(1, \frac{\lambda_{\max}(\bar{\mathbf{V}}^{(t+1)})}{\text{Tr}(\bar{\mathbf{V}}^{(t+1)})} + \tau^{(t+1)}\right)$ ;  
 11:  $t = t + 1$ ;  
 12: **end while**  
 13: Obtain  $\Phi$  by decompose  $\bar{\mathbf{V}}$ .  
 14: **Output:**  $\Phi$ .

---

Problem (28) is an SDP problem and can be solved by the CVX tool [38]. The procedure for optimizing RIS reflecting coefficients is summarized in Algorithm 1.

### C. Antenna Position Design

With fixed  $\mathbf{R}$  and  $\Phi$ , the optimization problem can be further reformulated as

$$\max_{\tilde{\mathbf{t}}} \min_{l \in \mathcal{L}} \mathbf{a}^H(\theta_l) \Phi \mathbf{H}(\tilde{\mathbf{t}}) \mathbf{R} \mathbf{H}(\tilde{\mathbf{t}})^H \Phi^H \mathbf{a}(\theta_l) \quad (29a)$$

$$\text{s.t. SINR}_k \geq \Gamma, \quad (29b)$$

$$\|\mathbf{t}_k - \mathbf{t}_q\|_2 \geq D, k \neq q, \quad (29c)$$

$$\tilde{\mathbf{t}} \in \mathcal{C}, \quad (29d)$$

which is a non-convex problem owing to the complex form of the objective function and the non-convex constraints. To deal with the max-min objective function, we first introduce an auxiliary variable  $\chi$ , and the problem can be reformulated as

$$\max_{\tilde{\mathbf{t}}} \chi \quad (30a)$$

$$\text{s.t. } \mathbf{a}^H(\theta_l) \Phi \mathbf{H}(\tilde{\mathbf{t}}) \mathbf{R} \mathbf{H}(\tilde{\mathbf{t}})^H \Phi^H \mathbf{a}(\theta_l) \geq \chi, \quad l \in \mathcal{L}, \quad (30b)$$

$$\text{SINR}_k \geq \Gamma, \quad (30c)$$

$$\|\mathbf{t}_k - \mathbf{t}_q\|_2 \geq D, k \neq q, \quad (30d)$$

$$\tilde{\mathbf{t}} \in \mathcal{C}. \quad (30e)$$

The main challenges in solving Problem (30) lie in the complicated expressions of  $\mathbf{H}(\tilde{\mathbf{t}})$ ,  $\mathbf{h}_{1,k}(\tilde{\mathbf{t}})$  and the tight coupling of  $\{\mathbf{t}_m\}_{m=1}^M$ . To this end, we aim to solve Problem (30) in an alternating manner. Specifically, we solve  $M$  subproblems of (30), which respectively optimize one transmit MA position  $\mathbf{t}_m$ , with all the other variables being fixed. The developed alternating optimization algorithm can obtain a locally suboptimal solution for (30) by solving the above  $M$  subproblems alternately.

We next consider the optimization of  $\mathbf{t}_m$  with given  $\{\mathbf{t}_q\}_{q \neq m}$ . For constraint (24b), we first rewrite the SINR constraint with respect to the  $k$ -th user as

$$\mathbf{h}_k^H [(1 + \Gamma^{-1}) \mathbf{R}_k - \mathbf{R}] \mathbf{h}_k \geq \sigma^2. \quad (31)$$

Since the antenna position  $\mathbf{t}_m$  is only related to  $\mathbf{g}(\mathbf{t}_m)$ , we can convert constraint (31) to a more tractable form,

$$(\mathbf{p}_k^H \mathbf{G}(\tilde{\mathbf{t}}) + \mathbf{q}_k^H \mathbf{G}_k(\tilde{\mathbf{t}})) \tilde{\mathbf{R}}_k (\mathbf{G}(\tilde{\mathbf{t}})^H \mathbf{p}_k + \mathbf{G}_k(\tilde{\mathbf{t}})^H \mathbf{q}_k) \geq \sigma^2, \quad (32)$$

where  $\mathbf{p}_k^H = \mathbf{h}_{1,k}^H \Phi \mathbf{F}(\mathbf{r})^H \Sigma$  and  $\mathbf{q}_k^H = \mathbf{1}^H \Sigma_k$  are invariant to  $\tilde{\mathbf{t}}$ . Define  $x_{k,q} = \mathbf{p}_k^H \mathbf{g}(\mathbf{t}_q) + \mathbf{q}_k^H \mathbf{g}_k(\mathbf{t}_q)$ ,  $q = 1, 2, \dots, M$ , constraint (32) can be recast as

$$\underbrace{\left[ \tilde{\mathbf{R}}_k \right]_{n,n}}_{\tilde{I}(\mathbf{t}_m)} |x_{k,m}|^2 + 2\Re\{\tilde{a}_k x_{k,m}\} \geq \sigma^2 - \tilde{b}_k, \quad (33)$$

where  $\tilde{a}_k$  and  $\tilde{b}_k$  are given at the bottom of the next page. It is worth noting that  $x_{k,m}$  is the optimization variable related to the antenna position  $\mathbf{t}_m$ ,  $\tilde{a}_k$  and  $\tilde{b}_k$  are variables invariant to  $\mathbf{t}_m$ . To fully reveal the optimization variable  $\mathbf{t}_m$  in the current form of constraint (33), we expand the left-hand-side of constraint (33) in (36), as shown at the bottom of the next page. In (36),  $\mathbf{P}_k \triangleq \mathbf{p}_k \mathbf{p}_k^H$ ,  $\mathbf{Q}_k \triangleq \mathbf{q}_k \mathbf{q}_k^H$ .

However,  $\tilde{I}(\mathbf{t}_m)$  is neither concave nor convex over  $\mathbf{t}_m$ , making constraint (33) still non-convex and thus intractable. To tackle this problem, we use the SCA method and transform the non-convex constraint. Specifically, by using the Taylor's theorem, we can construct a quadratic surrogate function that serves as a strict convex constraint to (33). With given local point  $\mathbf{t}_m^{(i)} \in \mathbb{R}^2$  in the  $i$ -th iteration, a lower bound can be obtained as  $\tilde{I}(\mathbf{t}_m) \geq \tilde{I}(\mathbf{t}_m^{(i)}) + \nabla \tilde{I}(\mathbf{t}_m^{(i)})^T (\mathbf{t}_m - \mathbf{t}_m^{(i)}) - \frac{\tilde{\delta}_m^{(i)}}{2} (\mathbf{t}_m - \mathbf{t}_m^{(i)})^T (\mathbf{t}_m - \mathbf{t}_m^{(i)})$ , where  $\tilde{\delta}_m^{(i)}$  is a positive real number which satisfies  $\tilde{\delta}_m^{(i)} \mathbf{I}_2 \succeq \nabla^2 \tilde{I}(\mathbf{t}_m)$ . The gradient vector  $\nabla \tilde{I}(\mathbf{t}_m)$  and the Hessian matrix  $\nabla^2 \tilde{I}(\mathbf{t}_m)$  are given in Appendix B. According to Appendix B and  $\|\nabla^2 \tilde{I}(\mathbf{t}_m)\|_2 \mathbf{I}_2 \succeq \nabla^2 \tilde{I}(\mathbf{t}_m)$ , we obtain the  $\tilde{\delta}_m^{(i)}$  as follows:

$$\begin{aligned} \tilde{\delta}_m^{(i)} &= \frac{64\pi^2}{\lambda} \left[ \sum_{i=1}^{L_t-1} \sum_{j=i+1}^{L_t} \left[ \tilde{\mathbf{R}}_k \right]_{m,m} \left| [\mathbf{Q}_k]_{i,j} \right| \right. \\ &\quad + \sum_{i=1}^{L_t-1} \sum_{j=i+1}^{L_t} \left[ \tilde{\mathbf{R}}_k \right]_{m,m} \left| [\mathbf{P}_k]_{i,j} \right| \\ &\quad \left. + \sum_{i=1}^{L_t} \sum_{j=1}^{L_t} \left[ \tilde{\mathbf{R}}_k \right]_{m,m} \left| [\mathbf{p}_k]_i \right| \left| [\mathbf{q}_k]_j \right| \right] \\ &\quad + \frac{16\pi^2}{\lambda} \left[ \sum_{i=1}^{L_t} |\tilde{a}_k| \left| [\mathbf{p}_k]_i \right| + \sum_{j=1}^{L_t} |\tilde{a}_k| \left| [\mathbf{q}_k]_j \right| \right] \\ &\geq \|\nabla^2 \tilde{I}(\mathbf{t}_m)\|_F \stackrel{(a)}{\geq} \|\nabla^2 \tilde{I}(\mathbf{t}_m)\|_2, \end{aligned} \quad (37)$$

which satisfies  $\tilde{\delta}_m^{(i)} \mathbf{I}_2 \succeq \|\nabla^2 \tilde{I}(\mathbf{t}_m)\|_2 \mathbf{I}_2 \succeq \nabla^2 \tilde{I}(\mathbf{t}_m)$ . The inequality marked by (a) holds because  $\|\nabla^2 \tilde{I}(\mathbf{t}_m)\|_F = \sqrt{\sum_{i=1}^2 \sigma_i^2(\nabla^2 \tilde{I}(\mathbf{t}_m))} \geq \sigma_{\max}(\nabla^2 \tilde{I}(\mathbf{t}_m)) = \|\nabla^2 \tilde{I}(\mathbf{t}_m)\|_2$ ,

where  $\sigma_i(\nabla^2 \bar{I}(\mathbf{t}_m))$  are the singular values of  $\nabla^2 \bar{I}(\mathbf{t}_m)$ . Thus we can rewrite constraint (33) as

$$\begin{aligned} \bar{I}(\mathbf{t}_m) &\geq \bar{I}(\mathbf{t}_m^{(i)}) + \nabla \bar{I}(\mathbf{t}_m^{(i)})^T (\mathbf{t}_m - \mathbf{t}_m^{(i)}) \\ &\quad - \frac{\tilde{\delta}_m^{(i)}}{2} (\mathbf{t}_m - \mathbf{t}_m^{(i)})^T (\mathbf{t}_m - \mathbf{t}_m^{(i)}) \\ &= -\frac{\tilde{\delta}_m^{(i)}}{2} \mathbf{t}_m^T \mathbf{t}_m + \left( \nabla \bar{I}(\mathbf{t}_m^{(i)}) + \tilde{\delta}_m^{(i)} \mathbf{t}_m^{(i)} \right)^T \mathbf{t}_m \\ &\quad + \underbrace{\bar{I}(\mathbf{t}_m^{(i)}) - \frac{\tilde{\delta}_m^{(i)}}{2} (\mathbf{t}_m^{(i)})^T \mathbf{t}_m^{(i)} - \nabla \bar{I}(\mathbf{t}_m^{(i)})^T \mathbf{t}_m^{(i)}}_{\text{const}} \\ &\geq \sigma^2 - \tilde{b}_k. \end{aligned} \quad (38)$$

Next, we tackle the non-convexity of constraint (30a). Define  $\mathbf{d}^H(\theta_l) = \mathbf{a}^H(\theta_l) \Phi \mathbf{F}(\mathbf{r})^H \Sigma$ , (30a) can be rewritten as

$$\begin{aligned} &\mathbf{a}^H(\theta_l) \Phi \mathbf{H}(\tilde{\mathbf{t}}) \mathbf{R} \mathbf{H}(\tilde{\mathbf{t}})^H \Phi^H \mathbf{a}(\theta_l) \\ &= \underbrace{\mathbf{d}^H(\theta_l) \mathbf{A}(\mathbf{t}_m) \mathbf{d}(\theta_l) + \mathbf{R}(n, n) |\mathbf{d}^H(\theta_l) \mathbf{g}(\mathbf{t}_m)|^2}_{I(\mathbf{t}_m)} \\ &\quad + \mathbf{d}^H(\theta_l) \mathbf{B}_n \mathbf{d}(\theta_l) \geq \chi, \end{aligned} \quad (39)$$

where  $\mathbf{A}(\mathbf{t}_m)$  is a linear function of  $\mathbf{g}(\mathbf{t}_m)$  and  $\mathbf{B}_n$  is a constant matrix independent of  $\mathbf{t}_m$ , which is defined in (40) and (41) respectively at the bottom of the next page. Since  $I(\mathbf{t}_m)$  can be lower bounded by its first-order Taylor expansion, we apply the SCA method and the non-convex constraint (39) can be rewritten as

$$\begin{aligned} &2 \underbrace{[\mathbf{R}]_{m,m} \Re \left\{ \mathbf{g}(\mathbf{t}_m^{(i)})^H \mathbf{d}_l(\theta) \mathbf{d}_l(\theta)^H \mathbf{g}(\mathbf{t}_m) \right\}}_{\bar{I}(\mathbf{t}_m)} + \mathbf{d}^H(\theta_l) \mathbf{A}(\mathbf{t}_m) \mathbf{d}(\theta_l) \\ &\geq \chi - \mathbf{d}^H(\theta_l) \mathbf{B}_n \mathbf{d}(\theta_l) + [\mathbf{R}]_{m,m} \left| \mathbf{d}(\theta_l)^H \mathbf{g}(\mathbf{t}_m^{(i)}) \right|^2, \end{aligned} \quad (42)$$

where  $\bar{I}(\mathbf{t}_m)$  is a linear function of  $\mathbf{g}(\mathbf{t}_m)$ , though it is still neither concave nor convex over  $\mathbf{t}_m$ . Analogous to (38), we can construct a second-order Taylor expansion-based concave lower bound for  $\bar{I}(\mathbf{t}_m)$ . For ease of exposition, we define  $\mathbf{b}_1^T \triangleq 2[\mathbf{R}]_{m,m} \mathbf{g}(\mathbf{t}_m^{(i)})^H \mathbf{d}_l(\theta) \mathbf{d}_l(\theta)^H$ ,  $\mathbf{b}_2^T \triangleq 2 \sum_{q=1, q \neq m}^M ([\mathbf{R}]_{m,q} \mathbf{g}(\mathbf{t}_q)^H) \mathbf{d}(\theta_l) \mathbf{d}^H(\theta_l)$  and  $\mathbf{b} = \mathbf{b}_1 + \mathbf{b}_2$ . Thus  $\bar{I}(\mathbf{t}_m)$  can be rewritten as

$$\begin{aligned} \bar{I}(\mathbf{t}_m) &= \Re \left\{ 2[\mathbf{R}]_{m,m} \mathbf{g}(\mathbf{t}_m^{(i)})^H \mathbf{d}_l(\theta) \mathbf{d}_l(\theta)^H \mathbf{g}(\mathbf{t}_m) \right\} \\ &\quad + \Re \left\{ 2\mathbf{d}^H(\theta_l) \sum_{q=1, q \neq n}^M (\mathbf{R}(n, q) \mathbf{g}(\mathbf{t}_q)^H) \mathbf{d}(\theta_l) \mathbf{g}(\mathbf{t}_m) \right\} \\ &= \Re \left\{ \mathbf{b}_1^T \mathbf{g}(\mathbf{t}_m) + \mathbf{b}_2^T \mathbf{g}(\mathbf{t}_m) \right\} \\ &= \Re \left\{ \mathbf{b}^T \mathbf{g}(\mathbf{t}_m) \right\} \\ &= \sum_{k=1}^{L_t} |[b]_k| \cos(\varrho^k(\mathbf{t}_m)), \end{aligned} \quad (43)$$

where  $\varrho^k(\mathbf{t}_m) \triangleq 2\pi \rho_t^k(\mathbf{t}_m) / \lambda + \angle [b]_k$ . In a similar way, we can calculate the the gradient vector  $\nabla \bar{I}(\mathbf{t}_m)$  and the Hessian matrix  $\nabla^2 \bar{I}(\mathbf{t}_m)$  of  $\bar{I}(\mathbf{t}_m)$ , which are omitted for simplicity.

$$\tilde{a}_k = \sum_{q=1, q \neq m}^M [\tilde{\mathbf{R}}_k]_{n,q} x_{k,q}^* \quad (34)$$

$$\tilde{b}_k = \sum_{p=1, p \neq m}^M \left( \sum_{q=1, q \neq m}^{p-1} 2\Re \{ [\tilde{\mathbf{R}}_k]_{p,q} x_{k,p} x_{k,q}^* \} + [\tilde{\mathbf{R}}_k]_{p,p} |x_{k,p}|^2 \right) \quad (35)$$

$$\begin{aligned} \tilde{I}(\mathbf{t}_m) &= [\tilde{\mathbf{R}}_k]_{m,m} (\mathbf{g}_k(\mathbf{t}_m)^H \mathbf{Q}_k \mathbf{g}_k(\mathbf{t}_m) + \mathbf{g}(\mathbf{t}_m)^H \mathbf{P}_k \mathbf{g}(\mathbf{t}_m) + 2\Re \{ \mathbf{p}_k^H \mathbf{g}(\mathbf{t}_m) \mathbf{g}_k(\mathbf{t}_m)^H \mathbf{q}_k \}) + 2\Re \{ \tilde{a}_k \mathbf{p}_k^H \mathbf{g}(\mathbf{t}_m) + \tilde{a}_k \mathbf{q}_k^H \mathbf{g}_k(\mathbf{t}_m) \} \\ &= 2 \sum_{i=1}^{L_t^k-1} \sum_{j=i+1}^{L_t^k} 2 [\tilde{\mathbf{R}}_k]_{m,m} |[\mathbf{Q}_k]_{i,j}| \cos \left( \frac{2\pi}{\lambda} (\rho_{t,k}^i(\mathbf{t}_m) - \rho_{t,k}^j(\mathbf{t}_m)) + \angle [\mathbf{Q}_k]_{i,j} \right) + \sum_{i=1}^{L_t^k} [\tilde{\mathbf{R}}_k]_{m,m} |[\mathbf{Q}_k]_{i,i}| \\ &\quad + 2 \sum_{i=1}^{L_t-1} \sum_{j=i+1}^{L_t} [\tilde{\mathbf{R}}_k]_{m,m} |[\mathbf{P}_k]_{i,j}| \cos \left( \frac{2\pi}{\lambda} (\rho_t^i(\mathbf{t}_m) - \rho_t^j(\mathbf{t}_m)) + \angle [\mathbf{P}_k]_{i,j} \right) + \sum_{i=1}^{L_t} [\tilde{\mathbf{R}}_k]_{m,m} |[\mathbf{P}_k]_{i,i}| \\ &\quad + 2 \sum_{i=1}^{L_t} \sum_{j=1}^{L_t^k} [\tilde{\mathbf{R}}_k]_{m,m} |[p_k]_i| |[q_k]_j| \cos \left( \frac{2\pi}{\lambda} (\rho_t^i(\mathbf{t}_m) - \rho_{t,k}^j(\mathbf{t}_m)) + \angle [q_k]_j - \angle [p_k]_i \right) \\ &\quad + 2 \sum_{i=1}^{L_t} |\tilde{a}_k| |[p_k]_i| \cos \left( \frac{2\pi}{\lambda} \rho_t^i(\mathbf{t}_m) - \angle [p_k]_i + \angle \tilde{a}_k \right) + 2 \sum_{j=1}^{L_t^k} |\tilde{a}_k| |[q_k]_j| \cos \left( \frac{2\pi}{\lambda} \rho_{t,k}^j(\mathbf{t}_m) - \angle [q_k]_j + \angle \tilde{a}_k \right) \end{aligned} \quad (36)$$

Hence, we can obtain the  $\bar{\delta}_m^{(i)}$  as follows:

$$\bar{\delta}_m^{(i)} = \frac{8\pi^2}{\lambda^2} \sum_{k=1}^{L_r} |[\mathbf{b}]_k|, \quad (44)$$

which satisfies  $\bar{\delta}_m^{(i)} \mathbf{I}_2 \succeq \|\nabla^2 \bar{I}(\mathbf{t}_m)\|_2 \mathbf{I}_2 \succeq \nabla^2 \bar{I}(\mathbf{t}_m)$ . Thus, we can rewrite constraint (42) as

$$\begin{aligned} \bar{I}(\mathbf{t}_m) &\geq \bar{I}(\mathbf{t}_m^{(i)}) + \nabla \bar{I}(\mathbf{t}_m^{(i)})^T (\mathbf{t}_m - \mathbf{t}_m^{(i)}) \\ &\quad - \frac{\delta_n^{(i)}}{2} (\mathbf{t}_m - \mathbf{t}_m^{(i)})^T (\mathbf{t}_m - \mathbf{t}_m^{(i)}) \\ &= -\frac{\delta_n^{(i)}}{2} \mathbf{t}_m^T \mathbf{t}_m + \left( \nabla \bar{I}(\mathbf{t}_m^{(i)}) + \delta_n^{(i)} \mathbf{t}_m^{(i)} \right)^T \mathbf{t}_m \\ &\quad + \underbrace{\bar{I}(\mathbf{t}_m^{(i)}) - \frac{\delta_n^{(i)}}{2} (\mathbf{t}_m^{(i)})^T \mathbf{t}_m^{(i)} - \nabla \bar{I}(\mathbf{t}_m^{(i)})^T \mathbf{t}_m^{(i)}}_{\text{const}} \\ &\geq \chi - \mathbf{d}^H(\theta_l) \mathbf{B}_m \mathbf{d}(\theta_l) + [\mathbf{R}]_{m,m} \left| \mathbf{d}_l(\theta)^H \mathbf{g}(\mathbf{t}_m^{(i)}) \right|^2. \end{aligned} \quad (45)$$

Finally, constraint (30d) can be relaxed at the given point  $\mathbf{t}_m^{(i)}$  as follows according to [20]

$$\|\mathbf{t}_m - \mathbf{t}_q\|_2 \geq \frac{1}{\|\mathbf{t}_m^{(i)} - \mathbf{t}_q\|_2} (\mathbf{t}_m^{(i)} - \mathbf{t}_q)^T (\mathbf{t}_m - \mathbf{t}_q) \geq D. \quad (46)$$

Hence, the antenna position design problem can be reformulated as

$$\max_{\tilde{\mathbf{t}}} \chi \quad (47a)$$

$$\text{s.t.} \quad (41), (49), (50), (24d), \quad (47b)$$

which is a convex quadratically constrained problem (QCP) that can be solved efficiently by standard convex solvers such as CVX [38]. Based on the above discussions, the detailed procedures of the overall AO-based algorithm are summarized in Algorithm 2.

## V. SIMULATION RESULTS

In this section, we present simulation results to assess the performance of the proposed MA and RIS-aided ISAC systems. In the simulation setup, we assume that the BS is fixed at (0, 0) and RIS is located at (12 m, 16 m). The users are randomly distributed in the rectangle area between (20 m, 0) and (40 m, -20 m). We consider the geometry channel model, where the numbers of transmit and receive paths are the same, i.e.,  $L_t = L_r = L = 4$ . According to the aforementioned

### Algorithm 2 Alternating Optimization for Solving Problem (14)

- 1: **Input:**  $\Sigma, P_0, \sigma, M, N, L_r, L_t, \{\theta_i^r\}_{i=1}^{L_r}, \{\phi_i^r\}_{i=1}^{L_r}, \{\theta_j^t\}_{j=1}^{L_t}, \{\phi_j^t\}_{j=1}^{L_t}, \mathcal{C}, D, \epsilon_1, \epsilon_2$ .
- 2: **Initialize**  $\{\mathbf{t}_m\}_{m=1}^M$ .
- 3: **while** Increase of the minimum beampattern gain in (13) is above  $\epsilon_1$  **do**
- 4:   Obtain the optimal solution of  $\mathbf{R}$  with given  $\{\mathbf{t}_m\}_{m=1}^M$  by solving Problem (16).
- 5:   Obtain the optimal solution of  $\Phi$  by Algorithm 1.
- 6:   **for**  $n = 1 \rightarrow M$  **do**
- 7:     **while** Increase of the minimum beampattern gain in (13) is above  $\epsilon_2$  **do**
- 8:       Given  $\mathbf{R}, \Phi$ , solve Problem (47) to update  $\mathbf{t}_m$ .
- 9:     **end while**
- 10:   **end for**
- 11: **end while**
- 12: **Output:**  $\mathbf{R}, \Phi, \tilde{\mathbf{t}}$ .

system model, we consider LoS channel between the BS-RIS link and RIS-Use link. In addition, the PRMs of the LoS channels are modeled as  $\Sigma[1, 1] \sim \mathcal{CN}(0, K_0(\frac{d}{d_0})^{-\alpha} \kappa / (\kappa + 1))$  and  $\Sigma[p, p] \sim \mathcal{CN}(0, K_0(\frac{d}{d_0})^{-\alpha} / ((\kappa + 1)(L - 1)))$ ,  $p = 2, 3, \dots, L$ , where  $\kappa$  denotes the ratio of the average power for LoS paths to that for NLoS paths. The distance-dependent path-loss is modeled as  $K_0(\frac{d}{d_0})^{-\alpha}$ , where  $K_0 = -40$  dB is the average channel power gain at the reference distance  $d_0 = 1$  m and  $\alpha$  is the pathloss exponents. Since obstacles exist between the BS-Use links, we consider Rayleigh fading and an additional shadow fading with a standard deviation of 15 dB between the NLoS channels. Unless otherwise stated, the simulation parameters are set as follows: The number of MAs at the DFRC BS  $M = 8$ , the number of downlink users  $K = 2$ , the interested angles  $\{\theta_1, \theta_2, \dots, \theta_5\} = \{-60^\circ, -30^\circ, 0^\circ, 30^\circ, 60^\circ\}$ , the transmit power at the DFRC BS  $P_0 = 60$  dBm, the user SINR threshold  $\Gamma = 10$  dB, the noise power at the receive antenna  $\sigma_k^2 = -40$  dBm, the number paths  $L = 4$ , and the pathloss exponents of BS-RIS, RIS-CU, BS-CU channels of 2.5, 2.5, 3.5, respectively. All the results are averaged over 400 independent channel realizations.

### A. Convergence Behavior of the Proposed Algorithms

The convergence behavior of the proposed algorithm is shown in Fig. 3. As illustrated in Fig. 3, the minimum beampattern gains of all schemes increase with the iteration index and converge within 150 iterations, thus validating the

$$\mathbf{A}(\mathbf{t}_m) = \sum_{q=1, q \neq m}^M \left( [\mathbf{R}]_{m,q} \mathbf{g}(\mathbf{t}_m) \mathbf{g}(\mathbf{t}_q)^H + [\mathbf{R}]_{m,q}^* \mathbf{g}(\mathbf{t}_q) \mathbf{g}(\mathbf{t}_m)^H \right) \quad (40)$$

$$\mathbf{B}_m = \sum_{k=1, k \neq m}^M \left( \sum_{q=1, q \neq m}^{k-1} \left( [\mathbf{R}]_{k,q} \mathbf{g}(\mathbf{t}_k) \mathbf{g}(\mathbf{t}_q)^H + [\mathbf{R}]_{k,q}^* \mathbf{g}(\mathbf{t}_q) \mathbf{g}(\mathbf{t}_k)^H \right) + [\mathbf{R}]_{k,k} \mathbf{g}(\mathbf{t}_k) \mathbf{g}(\mathbf{t}_k)^H \right) \quad (41)$$



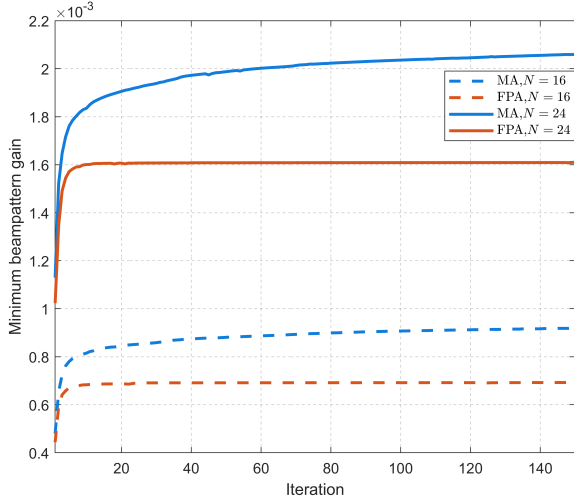


Fig. 3: Convergence behavior.

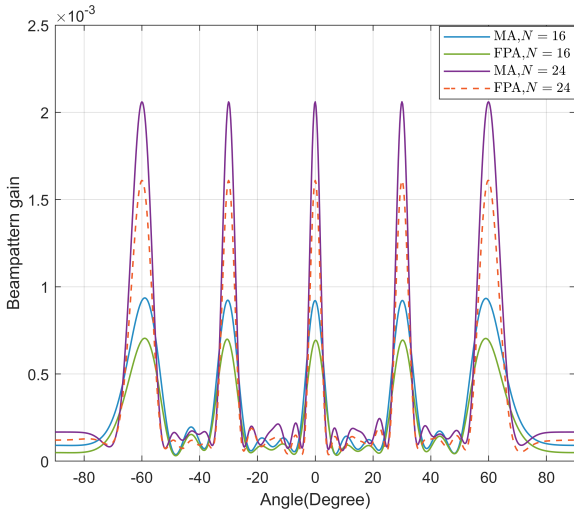


Fig. 4: The beampattern gains of different schemes.

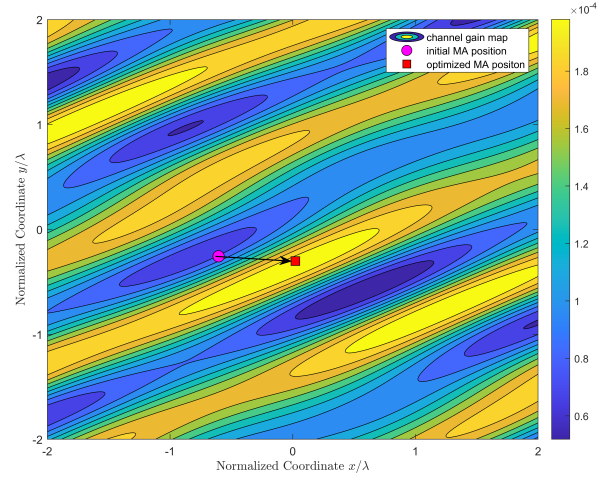
effectiveness of our proposed algorithm. In addition, the MA-aided schemes outperform its FPA-aided counterparts, but require more iterations to converge. This is owing to the procedure of antenna position optimization in our proposed algorithm.

### B. Beampattern at the RIS

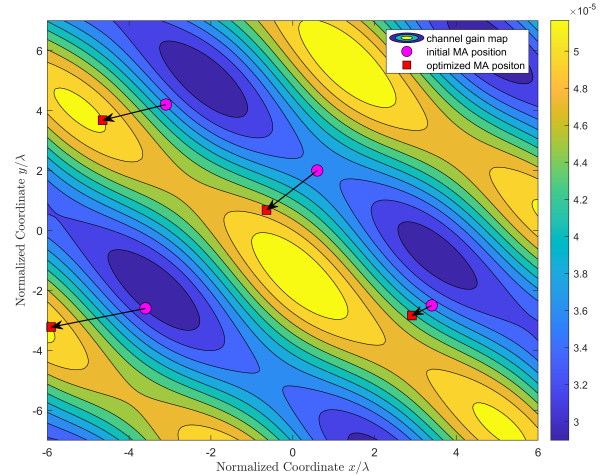
As depicted in Fig. 4, the values of beampattern gain in the direction of the interested angles in each scheme are approximately the same, which can be attributed to the principle of fairness inherent in the max-min optimization problem. In addition, the beampattern gain of the MA-aided scheme exceed its FPA-aided counterpart by approximately 25%, which reveals the advantage of the deployment of MAs at the DFRC BS, owing to its capacity of channel state configuration and array geometry reconstruction. Furthermore, the increase in the number of the RIS reflecting elements will

result in narrower main lobe of the beampattern, which means better directivity of the sensing function.

### C. Channel Characteristics under Antenna Position Optimization



(a)



(b)

Fig. 5: Examples for the channel power gain in the transmit region  $C_t$ : (a) Movement of a single antenna; (b) Movement of  $M = 4$  antennas.

To explore the effect of MA on improving the channel environment and array geometry, two channel implementations in which the channel gain of BS-RIS link versus the MA's position are presented in Fig. 5. To demonstrate the role of MA in improving the communication environment, Fig. 5(a) and Fig. 5(b) respectively present two implementations of channel gain enhancement via the BS-RIS chain as the antenna position changes. For convenience and clarity, the experiments set the number of antennas  $M$  to 1 and 4, respectively. In the single-antenna BS scenario, the RIS sensing angles  $\{\theta_1, \dots, \theta_L\}$  are set to  $\{0^\circ\}$  with user number  $K = 1$ . In the BS multi-antenna scenario with  $M = 4$ , the RIS sensing angles  $\{\theta_1, \dots, \theta_L\}$

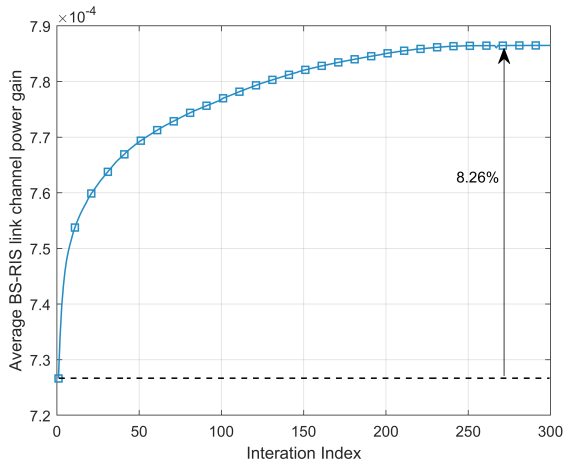


Fig. 6: Channel power gain of BS-RIS link versus iteration index

are set to  $\{-30^\circ, 0^\circ, 30^\circ\}$  with a service user number  $K = 2$ . To verify the superiority of the algorithm, the channel power gain of the BS-RIS link is defined as  $\|\mathbf{H}(\tilde{\mathbf{t}})\|^2$ , and the channel gain of the BS-RIS link is increased by 60% and 12% in the two implementations, respectively. Furthermore, it can be observed that in the case of  $M = 4$ , unlike the single antenna scenario, the positions of the MAs are not all optimized to the locations with the maximum channel gain. This is reasonable because the ISAC system needs to simultaneously perform sensing and communication, and the antenna arrays at certain positions can more easily form the desired waveform pattern [36]. Fig. 6 shows the curves of the BS-RIS link channel power gain versus the iteration index. It can be observed that the channel power gain gradually improves with the number of iterations, once again verifying the role of MA in improving the communication environment by mitigating small-scale fading caused by multipath effects.

We define the cross-correlation coefficient of the equivalent user channels  $\rho = \frac{1}{K(K-1)} \sum_{1 \leq k \neq q \leq K} \frac{|\mathbf{h}_k(\tilde{\mathbf{t}})^H \mathbf{h}_q(\tilde{\mathbf{t}})|}{\|\mathbf{h}_k(\tilde{\mathbf{t}})\|_2 \|\mathbf{h}_q(\tilde{\mathbf{t}})\|_2}$ . In Fig. 7, we present the average channel gain of user equivalent channel  $\|\mathbf{h}_k\|^2$  and cross-correlation coefficient  $\rho$  over iteration index. Interestingly, we find that during the procedure of the joint optimization, the variation of  $\|\mathbf{h}_k\|^2$  and  $\rho$  can be divided into two phases. In the first phase, the user channel gain decreases by approximately 0.2%, while the user channel similarity decreases by about 2.24%. Therefore, the gain in the ISAC system performance during this phase is partly attributed to the alleviation of multiuser interference, rather than merely enhancing the signal strength of individual users. In the second phase, the user channel gain increases by approximately 1.03%, and the channel similarity increases by about 1.52%. This can be attributed to the fact that the channel gain of the BS-RIS link is increasing along with the optimization process to enhance the sensing performance. Moreover, as more BS power is transferred to the BS-RIS link, it is reasonable to expect that both the gain and similarity of the user equivalent channel are also increasing during this phase.

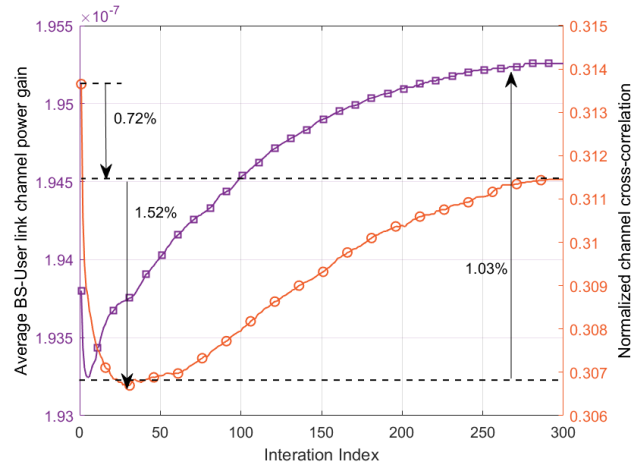


Fig. 7: Average user channel power gain and normalized cross-correlation versus iteration index.

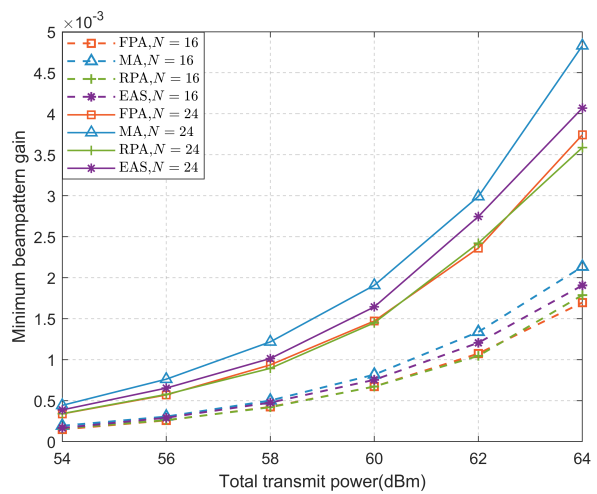


Fig. 8: Minimum beampattern gain versus transmit power  $P_0$ .

#### D. Performance Comparison with Benchmark Schemes

To comprehensively illustrate the advantages of MAs in enhancing the sensing and communication performance, we propose the following three baseline schemes:

- 1) **Fixed position antenna (FPA)**: The BS is equipped with a UPA based on FPA configuration, with  $M$  antennas spaced between interval of  $\frac{\lambda}{2}$ .
- 2) **Random position antenna (RPA)**: The BS is equipped with  $M$  antennas, which are randomly distributed within the transmit region  $\mathcal{C}$ , subject to a minimum distance  $D$  between each pair of antennas.
- 3) **Exhaustive antenna selection (EAS)**: The BS is equipped with an FPA-based UPA, consisting of  $2M$  antennas spaced at  $\frac{\lambda}{2}$  intervals. From these,  $M$  antennas are selected through an exhaustive search.

In Fig. 8, we illustrate the beampattern gain of the proposed and benchmark schemes versus the maximum transmit power  $P_0$ . Firstly, it can be clearly observed from Fig. 8 that the ISAC system equipped with  $N = 24$  RIS exhibits approxi-

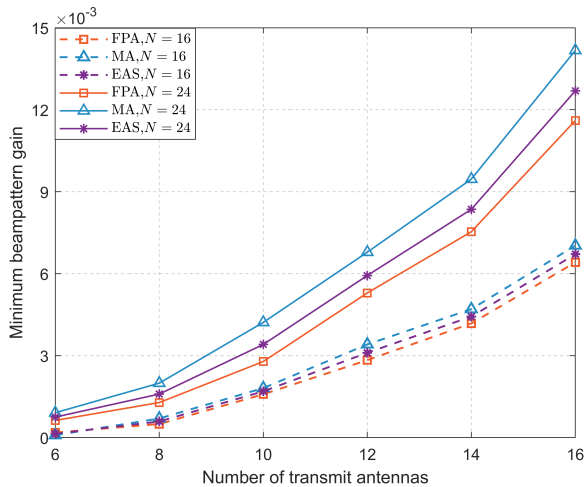


Fig. 9: Minimum beampattern gain versus the number of transmit antennas  $M$ .

mately a 110% significant performance improvement over the system with  $N = 16$  under three different transmit antenna configurations, demonstrating the importance of deploying RIS in ISAC systems for sensing dead zones. Additionally, MA scheme, which fully utilizes spatial DoFs, achieves about 24.6% performance gain over the FPA scheme in all scenarios by simultaneously improving the channel environment, suppressing multi-user interference, and optimizing the geometric characteristics of the antenna array. The EAS strategy falls between the MA and FPA schemes, showing an approximate 11.3% performance enhancement compared to the FPA.

Fig. 9 shows the minimum beampattern gain versus the number of transmit antennas. It shows that the beampattern gain increases in all schemes due to the spatial diversity gain and array gain introduced by additional antennas. Notably, when the number of antennas doubles from 6 to 12 in the MA-aided scheme with  $N = 24$ , the beampattern gain increases from  $0.91 \times 10^{-3}$  to  $6.78 \times 10^{-3}$ , achieving a gain of 653%. In contrast, as the transmit power increases from 58 dBm to 62 dBm in MA-aided scheme as in Fig. 8, the beampattern gain only rises from  $1.23 \times 10^{-3}$  to  $2.91 \times 10^{-3}$ . In other words, a 150% increase in transmit power only achieve a performance gain of 141%. This indicates that increasing the number of MAs can significantly enhance the sensing performance by leveraging the spatial DoFs.

The relationship between the minimum beampattern gain and the number of transmit paths is demonstrated in Fig. 10. It is worth noting that the sensing performance of MA-aided DFRC systems declines with the increase in  $L$ , which is contrary to the property that channel capacity tends to increase with the number of transmit paths [20]. This phenomenon can be attributed to the negative impact of electromagnetic wave scattering on sensing capabilities.

## VI. CONCLUSION

In this paper, we investigated an MA and RIS-aided ISAC system, where the DFRC BS is equipped with MAs to enhance both sensing and communication performance. Aiming

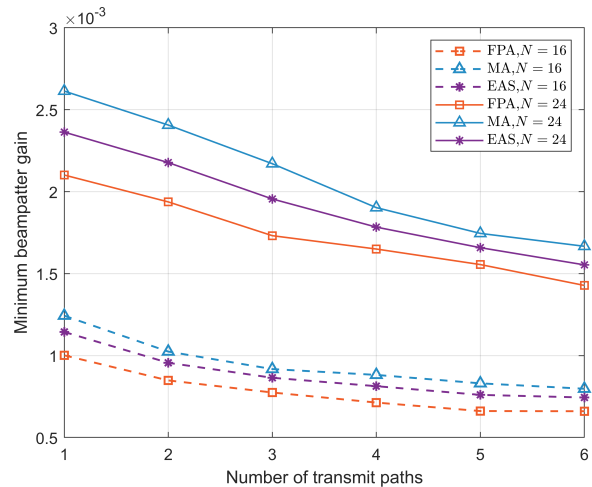


Fig. 10: Minimum beampattern gain versus the number of transmit paths  $L$ .

at maximizing the minimum beampattern gain at the RIS towards the desired sensing angles, we jointly optimized the transmit beamforming at the BS, the phase shifts of the RIS and the positions of the MAs, subject to the user SINR constraint and the transmit power constraint at the BS. Due to the highly non-convex nature of the resultant problem, we developed an AO-based algorithm utilizing SDR, SRCR, and SCA techniques. Specifically, the SRCR algorithm was utilized for optimizing the phase shifts at the RIS, owing to the potential nonconvergence characteristics caused by SDR. Simulation results illustrated significant advantages of the MA and RIS-aided system over other baseline schemes in ISAC systems. In addition, this paper meticulously discussed the variation in channel characteristics during the procedure of antenna position optimization. It is observed that the energy of the user channels initially decreases before increasing during the optimization process of the iterative algorithm, which is owing to the deployment of the RIS.

## APPENDIX A

Since the optimal solution  $\hat{\mathbf{R}}, \{\hat{\mathbf{R}}_k\}$  of Problem (17) are usually not of rank-one owing to the relaxation of constraint (16e), we construct the rank-one solution of Problem (16) with  $\tilde{\mathbf{R}}, \{\tilde{\mathbf{R}}_k\}$  as follows:

$$\tilde{\mathbf{R}} = \hat{\mathbf{R}}, \tilde{\mathbf{w}}_k = \left( \mathbf{h}_k^H \hat{\mathbf{R}}_k \mathbf{h}_k \right)^{-1/2} \hat{\mathbf{R}}_k \mathbf{h}_k, \tilde{\mathbf{R}}_k = \tilde{\mathbf{w}}_k \tilde{\mathbf{w}}_k^H, \quad (48)$$

$$\mathbf{h}_k^H \tilde{\mathbf{R}}_k \mathbf{h}_k = \mathbf{h}_k^H \tilde{\mathbf{w}}_k \tilde{\mathbf{w}}_k^H \mathbf{h}_k = \mathbf{h}_k^H \frac{\hat{\mathbf{R}}_k \mathbf{h}_k \mathbf{h}_k^H \hat{\mathbf{R}}_k}{\mathbf{h}_k^H \hat{\mathbf{R}}_k \mathbf{h}_k} \mathbf{h}_k = \mathbf{h}_k^H \hat{\mathbf{R}}_k \mathbf{h}_k. \quad (49)$$

Because of (48)(49), we can easily prove that constraint (16b) (16c) (16d) is true. According to Cauchy-Schwarz inequality we have,

$$\left( \mathbf{h}_k^H \hat{\mathbf{R}}_k \mathbf{h}_k \right) \left( \mathbf{v}^H \hat{\mathbf{R}}_k \mathbf{v} \right) \geq \left| \mathbf{v}^H \hat{\mathbf{R}}_k \mathbf{h}_k \right|^2, \quad (50)$$

$$\begin{aligned}
 \frac{\partial \tilde{I}(\mathbf{t}_m)}{\partial x_m} = & -\frac{4\pi}{\lambda} \sum_{i=1}^{L_t^k-1} \sum_{j=i+1}^{L_t^k} [\tilde{\mathbf{R}}_k]_{m,m} |[\mathbf{Q}_k]_{i,j}| \left( -\cos \phi_{k,i}^t \sin \theta_{k,i}^t + \cos \phi_{k,j}^t \sin \theta_{k,j}^t \right) \sin \left( \frac{2\pi}{\lambda} \left( \rho_{t,k}^i(\mathbf{t}_m) - \rho_{t,k}^j(\mathbf{t}_m) \right) + \angle[\mathbf{Q}_k]_{i,j} \right) \\
 & -\frac{4\pi}{\lambda} \sum_{i=1}^{L_t-1} \sum_{j=i+1}^{L_t} [\tilde{\mathbf{R}}_k]_{m,m} |[\mathbf{P}_k]_{i,j}| \left( -\cos \phi_i^t \sin \theta_i^t + \cos \phi_j^t \sin \theta_j^t \right) \sin \left( \frac{2\pi}{\lambda} \left( \rho_t^i(\mathbf{t}_m) - \rho_t^j(\mathbf{t}_m) \right) + \angle[\mathbf{P}_k]_{i,j} \right) \\
 & -\frac{4\pi}{\lambda} \sum_{i=1}^{L_t} \sum_{j=1}^{L_t^k} [\tilde{\mathbf{R}}_k]_{m,m} |[\mathbf{p}_k]_i| |[\mathbf{q}_k]_j| \left( -\cos \phi_{k,i}^t \sin \theta_{k,i}^t + \cos \phi_j^t \sin \theta_j^t \right) \sin \left( \frac{2\pi}{\lambda} \left( \rho_t^i(\mathbf{t}_m) - \rho_{t,k}^j(\mathbf{t}_m) \right) + \angle[\mathbf{q}_k]_j - \angle[\mathbf{p}_k]_i \right) \\
 & -\frac{4\pi}{\lambda} \sum_{i=1}^{L_t} |\tilde{a}_k| |[\mathbf{p}_k]_i| \cos \phi_i^t \sin \theta_i^t \sin \left( \frac{2\pi}{\lambda} \rho_t^i(\mathbf{t}_m) - \angle[\mathbf{p}_k]_i + \angle \tilde{a}_k \right) \\
 & -\frac{4\pi}{\lambda} \sum_{j=1}^{L_t^k} |\tilde{a}_k| |[\mathbf{q}_k]_j| \cos \phi_{k,j}^t \sin \theta_{k,j}^t \sin \left( \frac{2\pi}{\lambda} \rho_{t,k}^i(\mathbf{t}_m) - \angle[\mathbf{q}_k]_j + \angle \tilde{a}_k \right)
 \end{aligned} \tag{53}$$

$$\begin{aligned}
 \frac{\partial \tilde{I}(\mathbf{t}_m)}{\partial y_m} = & -\frac{4\pi}{\lambda} \sum_{i=1}^{L_t^k-1} \sum_{j=i+1}^{L_t^k} [\tilde{\mathbf{R}}_k]_{m,m} |[\mathbf{Q}_k]_{i,j}| \left( -\cos \theta_{k,i}^t + \cos \theta_{k,j}^t \right) \sin \left( \frac{2\pi}{\lambda} \left( \rho_{t,k}^i(\mathbf{t}_m) - \rho_{t,k}^j(\mathbf{t}_m) \right) + \angle[\mathbf{Q}_k]_{i,j} \right) \\
 & -\frac{4\pi}{\lambda} \sum_{i=1}^{L_t-1} \sum_{j=i+1}^{L_t} [\tilde{\mathbf{R}}_k]_{m,m} |[\mathbf{P}_k]_{i,j}| \left( -\cos \theta_i^t + \cos \theta_j^t \right) \sin \left( \frac{2\pi}{\lambda} \left( \rho_t^i(\mathbf{t}_m) - \rho_t^j(\mathbf{t}_m) \right) + \angle[\mathbf{P}_k]_{i,j} \right) \\
 & -\frac{4\pi}{\lambda} \sum_{i=1}^{L_t} \sum_{j=1}^{L_t^k} [\tilde{\mathbf{R}}_k]_{m,m} |[\mathbf{p}_k]_i| |[\mathbf{q}_k]_j| \left( -\cos \theta_{k,i}^t + \cos \theta_j^t \right) \sin \left( \frac{2\pi}{\lambda} \left( \rho_t^i(\mathbf{t}_m) - \rho_{t,k}^j(\mathbf{t}_m) \right) + \angle[\mathbf{q}_k]_j - \angle[\mathbf{p}_k]_i \right) \\
 & -\frac{4\pi}{\lambda} \sum_{i=1}^{L_t} |\tilde{a}_k| |[\mathbf{p}_k]_i| \cos \theta_i^t \sin \left( \frac{2\pi}{\lambda} \rho_t^i(\mathbf{t}_m) - \angle[\mathbf{p}_k]_i + \angle \tilde{a}_k \right) \\
 & -\frac{4\pi}{\lambda} \sum_{j=1}^{L_t^k} |\tilde{a}_k| |[\mathbf{q}_k]_j| \cos \theta_{k,j}^t \sin \left( \frac{2\pi}{\lambda} \rho_{t,k}^i(\mathbf{t}_m) - \angle[\mathbf{q}_k]_j + \angle \tilde{a}_k \right)
 \end{aligned} \tag{54}$$

so we can easily derive that

$$\mathbf{v}^H \left( \hat{\mathbf{R}}_k - \tilde{\mathbf{R}}_k \right) \mathbf{v} = \mathbf{v}^H \hat{\mathbf{R}}_k \mathbf{v} - \left( \mathbf{h}_k^H \hat{\mathbf{R}}_k \mathbf{h}_k \right)^{-1} \left| \mathbf{v}^H \hat{\mathbf{R}}_k \mathbf{h}_k \right|^2 \geq 0, \quad \iota_{k,i,j}^3(\mathbf{t}_m) = \frac{2\pi}{\lambda} \left( \rho_t^i(\mathbf{t}_m) - \rho_{t,k}^j(\mathbf{t}_m) \right) + \angle[\mathbf{q}_k]_j - \angle[\mathbf{p}_k]_i, \tag{51}$$

which means

$$\tilde{\mathbf{R}} - \sum_{k=1}^K \tilde{\mathbf{R}}_k = \hat{\mathbf{R}} - \sum_{k=1}^K \hat{\mathbf{R}}_k + \sum_{k=1}^K \left( \hat{\mathbf{R}}_k - \tilde{\mathbf{R}}_k \right) \succeq 0. \tag{52}$$

Combining (48),(52), we know that the  $\hat{\mathbf{R}}, \{\hat{\mathbf{R}}_k\}$  satisfies all the constraints in Problem (16), thus we can always reconstruct an equivalent rank-one solution and accordingly find the optimal solution to Problem (16).

#### APPENDIX B

The relative terms of gradient vector  $\nabla \tilde{I}(\mathbf{t}_m) = \left[ \frac{\partial \tilde{I}(\mathbf{t}_m)}{\partial x_m}, \frac{\partial \tilde{I}(\mathbf{t}_m)}{\partial y_m} \right]^T$  are given in (53)-(54). For convenience of expression, we define

$$\iota_{k,i,j}^1(\mathbf{t}_m) = \frac{2\pi}{\lambda} \left( \rho_{t,k}^i(\mathbf{t}_m) - \rho_{t,k}^j(\mathbf{t}_m) \right) + \angle[\mathbf{Q}_k]_{i,j}, \tag{55}$$

$$\iota_{k,i,j}^2(\mathbf{t}_m) = \frac{2\pi}{\lambda} \left( \rho_t^i(\mathbf{t}_m) - \rho_t^j(\mathbf{t}_m) \right) + \angle[\mathbf{P}_k]_{i,j}, \tag{56}$$

and relative terms of the Hessian matrix  $\nabla^2 \tilde{I}(\mathbf{t}_m) = \begin{bmatrix} \frac{\partial^2 \tilde{I}(\mathbf{t}_m)}{\partial x_m \partial x_m} & \frac{\partial^2 \tilde{I}(\mathbf{t}_m)}{\partial x_m \partial y_m} \\ \frac{\partial^2 \tilde{I}(\mathbf{t}_m)}{\partial y_m \partial x_m} & \frac{\partial^2 \tilde{I}(\mathbf{t}_m)}{\partial y_m \partial y_m} \end{bmatrix}$  are given in (60)-(62). Specifically,  $\frac{\partial^2 \tilde{I}(\mathbf{t}_m)}{\partial y_m \partial x_m} = \frac{\partial^2 \tilde{I}(\mathbf{t}_m)}{\partial x_m \partial y_m}$ , thus  $\frac{\partial^2 \tilde{I}(\mathbf{t}_m)}{\partial y_m \partial x_m}$  is omitted for simplicity.

#### REFERENCES

- [1] F. Liu, L. Zhou, C. Masouros, A. Li, W. Luo, and A. Petropulu, "Toward dual-functional radar-communication systems: Optimal waveform design," *IEEE Trans. Signal Process.*, vol. 66, pp. 4264–4279, Aug. 2018.
- [2] F. Liu, C. Masouros, A. P. Petropulu, H. Griffiths, and L. Hanzo, "Joint radar and communication design: Applications, state-of-the-art, and the road ahead," *IEEE Trans. Commun.*, vol. 68, pp. 3834–3862, Jun. 2020.

- [3] Y. Cui, F. Liu, X. Jing, and J. Mu, "Integrating sensing and communications for ubiquitous IoT: Applications, trends, and challenges," *IEEE Netw.*, vol. 35, pp. 158–167, Sep. 2021.
- [4] F. Liu, Y. Cui, C. Masouros, J. Xu, T. X. Han, Y. C. Eldar, and S. Buzzi, "Integrated sensing and communications: Toward dual-functional wireless networks for 6G and beyond," *IEEE J. Sel. Areas Commun.*, vol. 40, pp. 1728–1767, Jun. 2022.
- [5] I. F. Akyildiz, C. Han, Z. Hu, S. Nie, and J. M. Jornet, "Terahertz band communication: An old problem revisited and research directions for the next decade," *IEEE Trans. Commun.*, vol. 70, pp. 4250–4285, May 2022.
- [6] A. Faisal, H. Sameddeen, H. Dahrouj, T. Y. Al-Naffouri, and M.-S. Alouini, "Ultramassive MIMO systems at terahertz bands: Prospects and challenges," *IEEE Veh. Technol. Mag.*, vol. 15, pp. 33–42, Oct. 2020.
- [7] A. Hassanien, M. G. Amin, E. Aboutanios, and B. Himed, "Dual-function radar communication systems: A solution to the spectrum congestion problem," *IEEE Veh. Technol. Mag.*, vol. 36, pp. 115–126, Apr. 2019.
- [8] L. Zheng, M. Lops, Y. C. Eldar, and X. Wang, "Radar and communication coexistence: An overview: A review of recent methods," *IEEE Signal Process. Mag.*, vol. 36, pp. 85–99, Sep. 2019.
- [9] F. Liu, L. Zheng, Y. Cui, C. Masouros, A. P. Petropulu, H. Griffiths, and Y. C. Eldar, "Seventy years of radar and communications: The road from separation to integration," *IEEE Signal Process. Mag.*, vol. 40, pp. 106–121, Jul. 2023.
- [10] X. Liu, T. Huang, N. Shlezinger, Y. Liu, J. Zhou, and Y. C. Eldar, "Joint transmit beamforming for multiuser MIMO communications and MIMO radar," *IEEE Trans. Signal Process.*, vol. 68, pp. 3929–3944, Jun. 2020.
- [11] H. Hua, J. Xu, and T. X. Han, "Optimal transmit beamforming for integrated sensing and communication," *IEEE Trans. Veh. Technol.*, Mar. 2023.
- [12] J. Zhang, E. Björnson, M. Matthaiou, D. W. K. Ng, H. Yang, and D. J. Love, "Prospective multiple antenna technologies for beyond 5G," *IEEE J. Sel. Areas Commun.*, vol. 38, pp. 1637–1660, Jun. 2020.
- [13] C. Pan, H. Ren, K. Wang, J. F. Kolb, M. Elkashlan, M. Chen, M. Di Renzo, Y. Hao, J. Wang, A. L. Swindlehurst, *et al.*, "Reconfigurable intelligent surfaces for 6G systems: Principles, applications, and research directions," *IEEE Commun. Mag.*, vol. 59, pp. 14–20, Jun. 2021.
- [14] C. Pan, G. Zhou, K. Zhi, S. Hong, T. Wu, Y. Pan, H. Ren, M. Di Renzo,

$$\begin{aligned}
 \frac{\partial^2 \tilde{I}(\mathbf{t}_m)}{\partial y_m \partial y_m} = & -\frac{8\pi^2}{\lambda} \sum_{i=1}^{L_t^k-1} \sum_{j=i+1}^{L_t^k} [\tilde{\mathbf{R}}_k]_{m,m} |[\mathbf{Q}_k]_{i,j}| (-\cos \theta_{k,i}^t + \cos \theta_{k,j}^t)^2 \cos(\iota_{k,i,j}^1(\mathbf{t}_m)) \\
 & -\frac{8\pi^2}{\lambda} \sum_{i=1}^{L_t-1} \sum_{j=i+1}^{L_t} [\tilde{\mathbf{R}}_k]_{m,m} |[\mathbf{P}_k]_{i,j}| (-\cos \theta_i^t + \cos \theta_j^t)^2 \cos(\iota_{k,i,j}^2(\mathbf{t}_m)) \\
 & -\frac{8\pi^2}{\lambda} \sum_{i=1}^{L_t} \sum_{j=1}^{L_t^k} [\tilde{\mathbf{R}}_k]_{m,m} |[\mathbf{p}_k]_i| |[\mathbf{q}_k]_j| (-\cos \theta_{k,i}^t + \cos \theta_j^t)^2 \cos(\iota_{k,i,j}^3(\mathbf{t}_m)) \\
 & -\frac{8\pi^2}{\lambda} \sum_{i=1}^{L_t} |\tilde{a}_k| |[\mathbf{p}_k]_i| \cos^2 \theta_i^t \cos(\kappa_{k,i}^1(\mathbf{t}_m)) - \frac{8\pi^2}{\lambda} \sum_{j=1}^{L_t^k} |\tilde{a}_k| |[\mathbf{q}_k]_j| \cos^2 \theta_{k,j}^t \cos(\kappa_{k,j}^2(\mathbf{t}_m))
 \end{aligned} \tag{60}$$

$$\begin{aligned}
 \frac{\partial^2 \tilde{I}(\mathbf{t}_m)}{\partial x_m \partial x_m} = & -\frac{8\pi^2}{\lambda} \sum_{i=1}^{L_t^k-1} \sum_{j=i+1}^{L_t^k} [\tilde{\mathbf{R}}_k]_{m,m} |[\mathbf{Q}_k]_{i,j}| (-\cos \phi_{k,i}^t \sin \theta_{k,i}^t + \cos \phi_{k,j}^t \sin \theta_{k,j}^t)^2 \cos(\iota_{k,i,j}^1(\mathbf{t}_m)) \\
 & -\frac{8\pi^2}{\lambda} \sum_{i=1}^{L_t-1} \sum_{j=i+1}^{L_t} [\tilde{\mathbf{R}}_k]_{m,m} |[\mathbf{P}_k]_{i,j}| (-\cos \phi_i^t \sin \theta_i^t + \cos \phi_j^t \sin \theta_j^t)^2 \cos(\iota_{k,i,j}^2(\mathbf{t}_m)) \\
 & -\frac{8\pi^2}{\lambda} \sum_{i=1}^{L_t} \sum_{j=1}^{L_t^k} [\tilde{\mathbf{R}}_k]_{m,m} |[\mathbf{p}_k]_i| |[\mathbf{q}_k]_j| (-\cos \phi_{k,i}^t \sin \theta_{k,i}^t + \cos \phi_j^t \sin \theta_j^t)^2 \cos(\iota_{k,i,j}^3(\mathbf{t}_m)) \\
 & -\frac{8\pi^2}{\lambda} \sum_{i=1}^{L_t} |\tilde{a}_k| |[\mathbf{p}_k]_i| \cos^2 \phi_i^t \sin^2 \theta_i^t \cos(\kappa_{k,i}^1(\mathbf{t}_m)) - \frac{8\pi^2}{\lambda} \sum_{j=1}^{L_t^k} |\tilde{a}_k| |[\mathbf{q}_k]_j| \cos^2 \phi_{k,j}^t \sin^2 \theta_{k,j}^t \cos(\kappa_{k,j}^2(\mathbf{t}_m))
 \end{aligned} \tag{61}$$

$$\begin{aligned}
 \frac{\partial^2 \tilde{I}(\mathbf{t}_m)}{\partial x_m \partial y_m} = & -\frac{8\pi^2}{\lambda} \sum_{i=1}^{L_t^k-1} \sum_{j=i+1}^{L_t^k} [\tilde{\mathbf{R}}_k]_{m,m} |[\mathbf{Q}_k]_{i,j}| (-\cos \phi_{k,i}^t \sin \theta_{k,i}^t + \cos \phi_{k,j}^t \sin \theta_{k,j}^t) (-\cos \theta_{k,i}^t + \cos \theta_{k,j}^t) \cos(\iota_{k,i,j}^1(\mathbf{t}_m)) \\
 & -\frac{8\pi^2}{\lambda} \sum_{i=1}^{L_t-1} \sum_{j=i+1}^{L_t} [\tilde{\mathbf{R}}_k]_{m,m} |[\mathbf{P}_k]_{i,j}| (-\cos \phi_i^t \sin \theta_i^t + \cos \phi_j^t \sin \theta_j^t) (-\cos \theta_i^t + \cos \theta_j^t) \cos(\iota_{k,i,j}^2(\mathbf{t}_m)) \\
 & -\frac{8\pi^2}{\lambda} \sum_{i=1}^{L_t} \sum_{j=1}^{L_t^k} [\tilde{\mathbf{R}}_k]_{m,m} |[\mathbf{p}_k]_i| |[\mathbf{q}_k]_j| (-\cos \phi_{k,i}^t \sin \theta_{k,i}^t + \cos \phi_j^t \sin \theta_j^t) (-\cos \theta_{k,i}^t + \cos \theta_j^t) \cos(\iota_{k,i,j}^3(\mathbf{t}_m)) \\
 & -\frac{8\pi^2}{\lambda} \sum_{i=1}^{L_t} |\tilde{a}_k| |[\mathbf{p}_k]_i| \cos \phi_i^t \sin \theta_i^t \cos \theta_i^t \cos(\kappa_{k,i}^1(\mathbf{t}_m)) - \frac{8\pi^2}{\lambda} \sum_{j=1}^{L_t^k} |\tilde{a}_k| |[\mathbf{q}_k]_j| \cos \phi_{k,j}^t \sin \theta_{k,j}^t \cos \theta_{k,j}^t \cos(\kappa_{k,j}^2(\mathbf{t}_m))
 \end{aligned} \tag{62}$$

- A. L. Swindlehurst, R. Zhang, *et al.*, “An overview of signal processing techniques for ris/irs-aided wireless systems,” *IEEE J. Sel. Top. Signal Process.*, vol. 16, pp. 883–917, Aug. 2022.
- [15] S. Buzzi, E. Grossi, M. Lops, and L. Venturino, “Foundations of MIMO radar detection aided by reconfigurable intelligent surfaces,” *IEEE Trans. Signal Process.*, vol. 70, pp. 1749–1763, Mar. 2022.
- [16] R. Liu, M. Li, Y. Liu, Q. Wu, and Q. Liu, “Joint transmit waveform and passive beamforming design for RIS-aided DFRC systems,” *IEEE J. Sel. Areas Commun.*, vol. 16, pp. 995–1010, May 2022.
- [17] X. Song, D. Zhao, H. Hua, T. X. Han, X. Yang, and J. Xu, “Joint transmit and reflective beamforming for IRS-assisted integrated sensing and communication,” in *IEEE Wireless Commun. Networking Conf. WCNC*, pp. 189–194, IEEE, May 2022.
- [18] R. P. Sankar, S. P. Chepuri, and Y. C. Eldar, “Beamforming in integrated sensing and communication systems with reconfigurable intelligent surfaces,” *IEEE Trans. Wireless Commun.*, Sep. 2023.
- [19] X. Wang, Z. Fei, Z. Zheng, and J. Guo, “Joint waveform design and passive beamforming for RIS-assisted Dual-Functional Radar-Communication system,” *IEEE Trans. Veh. Technol.*, vol. 70, pp. 5131–5136, Apr. 2021.
- [20] W. Ma, L. Zhu, and R. Zhang, “MIMO capacity characterization for movable antenna systems,” *IEEE Trans. Wireless Commun.*, vol. 23, pp. 3392–3407, Apr. 2024.
- [21] L. Zhu, W. Ma, and R. Zhang, “Modeling and performance analysis for movable antenna enabled wireless communications,” *IEEE Trans. Wireless Commun.*, vol. 23, pp. 6234–6250, Jun. 2024.
- [22] L. Zhu, W. Ma, and R. Zhang, “Movable antennas for wireless communication: Opportunities and challenges,” *IEEE Commun. Mag.*, vol. 62, pp. 114–120, Jun. 2024.
- [23] W. Ma, L. Zhu, and R. Zhang, “Compressed sensing based channel estimation for movable antenna communications,” *IEEE Commun. Lett.*, vol. 27, pp. 2747–2751, Oct. 2023.
- [24] Z. Xiao, S. Cao, L. Zhu, Y. Liu, B. Ning, X.-G. Xia, and R. Zhang, “Channel estimation for movable antenna communication systems: A framework based on compressed sensing,” *IEEE Trans. Wireless Commun.*, Apr. 2024.
- [25] L. Zhu, W. Ma, B. Ning, and R. Zhang, “Movable-antenna enhanced multiuser communication via antenna position optimization,” *IEEE Trans. Wireless Commun.*, pp. 1–1, Dec. 2023.
- [26] L. Zhu, W. Ma, Z. Xiao, and R. Zhang, “Performance analysis and optimization for movable antenna aided wideband communications,” *arXiv preprint arXiv:2401.08974*, 2024.
- [27] Y. Wu, D. Xu, D. W. K. Ng, W. Gerstaecker, and R. Schober, “Movable antenna-enhanced multiuser communication: Optimal discrete antenna positioning and beamforming,” *arXiv preprint arXiv:2308.02304*, 2023.
- [28] Z. Cheng, N. Li, J. Zhu, X. She, C. Ouyang, and P. Chen, “Enabling secure wireless communications via movable antennas,” in *Proc. IEEE ICASSP*, pp. 9186–9190, IEEE, Mar. 2024.
- [29] G. Hu, Q. Wu, K. Xu, J. Si, and N. Al-Dhahir, “Secure wireless communication via movable-antenna array,” *IEEE Signal Process. Lett.*, Jan. 2024.
- [30] J. Tang, C. Pan, Y. Zhang, H. Ren, and K. Wang, “Secure MIMO communication relying on movable antennas,” *arXiv preprint arXiv:2403.04269*, Jan. 2024.
- [31] G. Hu, Q. Wu, K. Xu, J. Ouyang, J. Si, Y. Cai, and N. Al-Dhahir, “Fluid Antennas-Enabled Multiuser Uplink: A Low-Complexity Gradient Descent for Total Transmit Power Minimization,” *IEEE Commun. Lett.*, vol. 28, pp. 602–606, Mar. 2024.
- [32] X. Chen, B. Feng, Y. Wu, D. W. K. Ng, and R. Schober, “Joint beamforming and antenna movement design for moveable antenna systems based on statistical CSI,” in *Proc. IEEE GLOBECOM*, pp. 4387–4392, IEEE, Feb. 2023.
- [33] Y. Sun, H. Xu, C. Ouyang, and H. Yang, “Sum-rate optimization for RIS-aided multiuser communications with movable antenna,” *arXiv preprint arXiv:2311.06501*, 2023.
- [34] J. Ding, Z. Zhou, C. Wang, W. Li, L. Lin, and B. Jiao, “Secure Full-Duplex Communication via Movable Antennas,” *arXiv preprint arXiv:2403.20025*, 2024.
- [35] W. Ma, L. Zhu, and R. Zhang, “Multi-beam forming with movable-antenna array,” *IEEE Commun. Lett.*, vol. 28, pp. 697–701, Mar. 2024.
- [36] W. Ma, L. Zhu, and R. Zhang, “Movable Antenna Enhanced Wireless Sensing Via Antenna Position Optimization,” *arXiv preprint arXiv:2405.01215*, 2024.
- [37] W. Lyu, S. Yang, Y. Xiu, Z. Zhang, C. Assi, and C. Yuen, “Flexible Beamforming for Movable Antenna-Enabled Integrated Sensing and Communication,” *arXiv preprint arXiv:2405.10507*, 2024.
- [38] S. P. Boyd and L. Vandenberghe, *Convex optimization*. Cambridge university press, 2004.
- [39] J. Zuo, Y. Liu, C. Zhu, Y. Zou, D. Zhang, and N. Al-Dhahir, “Exploiting NOMA and RIS in Integrated Sensing and Communication,” *IEEE Trans. Veh. Technol.*, vol. 72, pp. 12941–12955, May 2023.